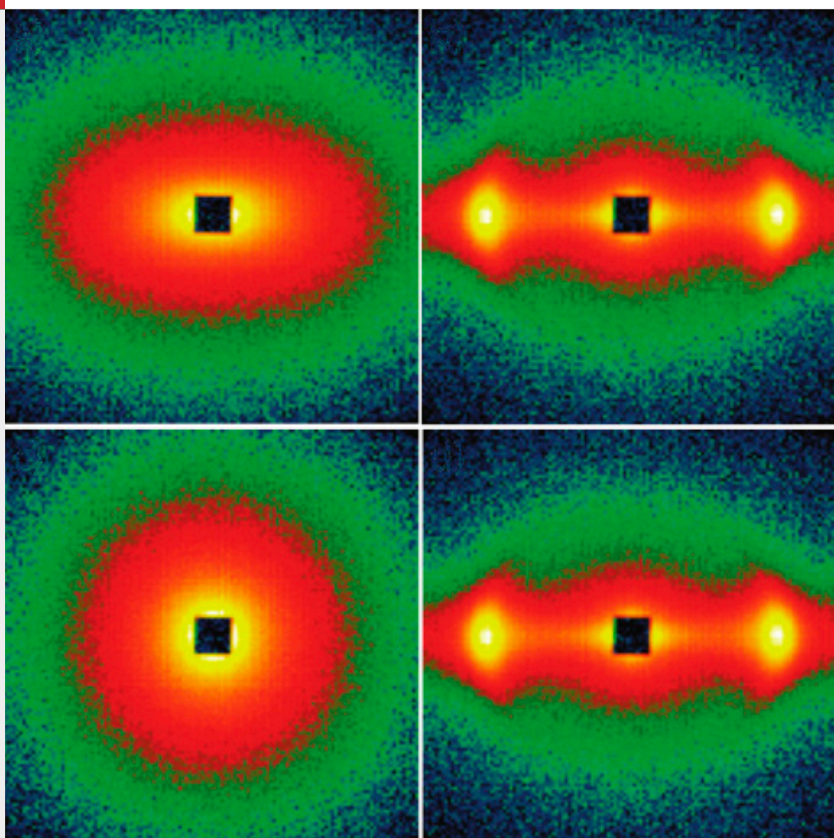
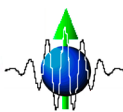


Number 45
March 2015

SWISS NEUTRON NEWS



Schweizerische Gesellschaft für Neutronenstreuung
Société Suisse pour la Diffusion des Neutrons
Swiss Neutron Scattering Society

EDITORIAL:

Editor: Swiss Neutron Scattering Society

Board for the Period October 2012 – October 2015:

President: Prof. Dr. Henrik Ronnow henrik.ronnow@epfl.ch

Board Members: Dr. M. Kenzelmann michel.kenzelmann@psi.ch
Dr. L.E. Bove livia.bove@epfl.ch
Dr. U. Gasser (secretary) urs.gasser@psi.ch

Honorary Members: Prof. Dr. W. Hälg, ETH Zürich (†)
Prof. Dr. K. A. Müller, IBM Rüschlikon and Univ. Zürich
Prof. Dr. A. Furrer, ETH Zürich and Paul Scherrer Institut

Auditors: Dr. K. Krämer, University of Berne
Dr. M. Zolliker, Paul Scherrer Institut

Address: Sekretariat SGN/SSDN
c/o Paul Scherrer Institut
WLG/018
5232 Villigen PSI, Switzerland
phone: +41 56 310 46 66
fax: +41 56 310 32 94
www: <http://sgn.web.psi.ch>

Bank Account: Postfinance: 50-70723-6 (BIC: POFICHBE)
IBAN: CH39 0900 0000 5007 0723 6

Printing: Paul Scherrer Institut

Circulation: 1600, 2 numbers per year

Copyright: SGN/SSDN and the respective authors

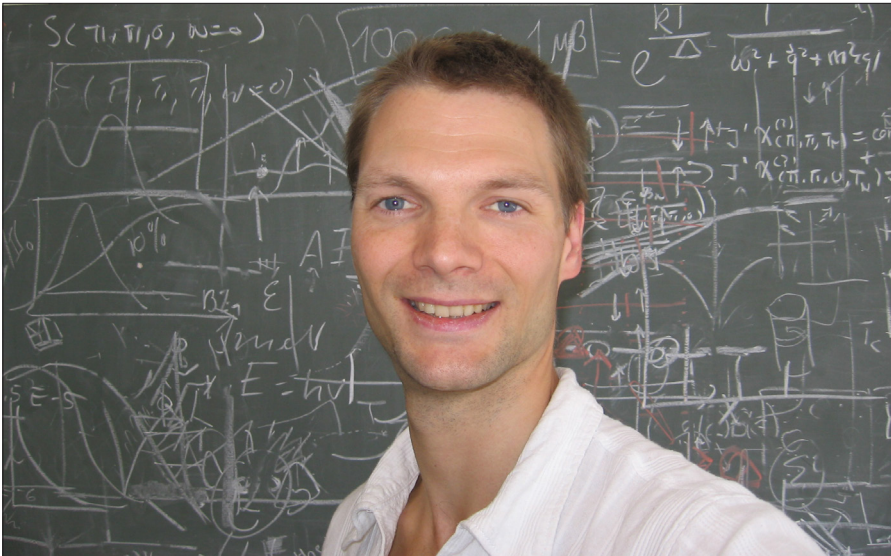
ON THE COVER:

2D SANS patterns of DPPC/Chol/DPPE-DTPA/Tm3+ bicelles, see the article "Design of magnetically responsive phospholipid bicelles towards switchable optical hydrogels" by M. Liebi et al.

Contents

- 2** The President's Page
- 4** Design of magnetically responsive phospholipid bicelles towards switchable optical hydrogels
- 14** Elucidating the biography of a proton in a proton conductor with neutrons and X-rays
- 23** Interplay of unconventional superconductivity and magnetism in the Q-phase of CeCoIn_5
- 31** Announcements
- 33** Minutes of the SGN/SSDN General Assembly 2014
- 38** Conferences

The President's Page



DEAR COLLEAGUES

Welcome to this issue of Neutron News. Firstly I would like to welcome the ENSA chairwoman Christian Alba-Simionesco and vice-chairman Ferenc Mezei, and simultaneously

take the opportunity to thank outgoing chairman Michael Steiner for his time at the helm.

Secondly, I have the pleasure of announcing a partnership between Switzerland and the Laboratory for Magnetism and Neutron

Diffraction (MDN) from INAC, CEA-Grenoble, who as a so-called collaborating research group (CRG) operate the instruments D23 (single crystal diffractometer with polarization option), IN12 (cold neutron spectrometer with polarization option) and IN22 (thermal neutron spectrometer with polarization option) at the ILL reactor. This agreement builds on years of collaboration between MDN and Swiss neutron science groups and increases the Swiss access to these instruments, which perfectly complement the capabilities of instruments at SINQ. Access to these instruments will happen via the usual ILL proposal rounds.

On a personal note, my laboratory recently had a couple of experiments postponed due to technical difficulties at various neutron sources around the world. This is by absolutely no means a criticism to the neutron sources, which we are so grateful for operating and for providing beam-time. Neutron sources, neutron scattering instruments and sample environments are complex machines

and unforeseen difficulties are - difficult to foresee. I mention this because I would like to highlight how lucky we are that our national source – SINQ - is extremely stable and reliable.

Finally – in just before Neutron News goes to print – March 9th was a great evening for Swiss neutron science. The Swiss National Council approved with dominant majority the budget for Swiss participation to construction and operation of ESS until 2026. Bundesrat Schneider-Ammann and representatives of the consulting commissions presented our case with very strong arguments, which were prepared extremely well by Martin Steinacher and his team at SBFi. We are truly grateful for their continued recognition and support. It is now our turn to make this a thundering success.

Ganbatte!
Henrik M. Ronnow

Design of magnetically responsive phospholipid bicelles towards switchable optical hydrogels

Marianne Liebi^{1,2}, Simon Kuster¹, Joachim Kohlbrecher³, Takashi Ishikawa⁴, Peter Walde⁵,
Erich J. Windhab¹ and Peter Fischer¹

¹ *Institute of Food, Nutrition and Health, ETH Zurich, Schmelzbergstrasse 9, 8092 Zurich, Switzerland*

² *Laboratory for Macromolecules and Bioimaging, Paul Scherrer Institute, 5232 Villigen PSI, Switzerland*

³ *Laboratory for Neutron Scattering, Paul Scherrer Institute, 5232 Villigen PSI, Switzerland*

⁴ *Biomolecular Research Laboratory, Paul Scherrer Institute, 5232 Villigen PSI, Switzerland*

⁵ *Department of Materials, ETH Zurich, Wolfgang-Pauli-Strasse 10, 8093 Zurich, Switzerland*

ABSTRACT

With the goal of producing smart hydrogels, magnetically alignable bicelles were embedded into a gelatin matrix, generating a magnetically switchable structure, which can reversibly be locked by lowering the temperature. Bicelles are a self-assembled structure based on phospholipids with a disk-like shape. The bicelles studied in this work are based on mixtures of two phospholipids and complexed lanthanide ions to guarantee shape and magnetic alignability. As shown in this contribution, the optical anisotropy of the bicelles can be used as independent readout of the gel's

orientation and its gelation history. Isotropic birefringence implies lack of alignment of the bicelles meaning that gelation has occurred in absence of a magnetic field. On the other hand, anisotropic birefringence indicates that the gelation occurred in the magnetic field orienting the bicelles. In this work the design pathways for magnetically responsive bicelles towards a maximum magnetic alignability of the bicelles within a gelatin matrix are summarized.

Keywords: bicelles, hydrogel, gelatin, phospholipids, magnetic aligning, smart material

DESIGN PATHWAY FOR MAGNETICALLY RESPONSIVE BICELLES

Mesostructures responding to external triggers such as temperature, pH, light, electric, and, in our case, magnetic fields have the potential to be used as self-acting sensors, detectors, or switches [1-3]. Key features are a strong and well-defined response to the external trigger. A magnetic response is in most cases induced by the inclusion of magnetic nanoparticles into a gel matrix. Thus, the magnetic field response includes remote heating, opening and closure of pores, as well as swelling, shrinking, and bending behavior induced by the superparamagnetic particles [4-6]. We used magnetically aligned bicelles based on phospholipids as building blocks within a gelatin matrix to generate magnetically and thermally switchable anisotropic structures with orientation dependent optical properties, which can be used as smart detectors or switches.

Bicelles based on phospholipids are nanometer-sized aggregates shaped like a disk. They are composed of a planar phospholipid bilayer and a torus-like end cap made from phospholipids with larger head groups to allow the closure of the disk's rim. In Figure 1 the design of bicelles is shown schematically. Depending on molecular ratio, concentration, temperature, and other physico-chemical parameters the same molecules can either form bicelles or vesicles, i.e. self-closed bilayers. The bicelles studied here are based on mixtures from DMPC (1,2-dimyristoyl-*sn*-glycero-3-phosphocholine), cholesterol, and DMPE-DTPA (1,2-dimyristoyl-*sn*-glycero-3-phosphoe-

thanolamine-diethylenetriaminepentaacetate) with complexed lanthanide ions and embedded in 5 % (w/w) gelatin.

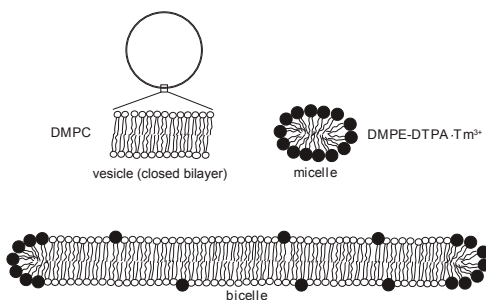


Figure 1: Bicelles composed out of the lamellar sheet of a bilayer (DMPC) and the end cap of micellar forming lanthanide-doped lipids (DMPE-DTPA). The different packing parameter (head diameter to tail diameter) of molecules in the lamellae and in the micelle is crucial for the shape, size and rim closure of the bicelle.

The magnetic alignment of single phospholipids due to their magnetic moment is extremely small and is ruled out by thermal fluctuations. The situation improves when phospholipids self-assemble in mesostructures such as lamellar sheets, thus bicelles, summing up the individual diamagnetic moments. The alignment of the bicelles in a magnetic field is due to the anisotropy of the diamagnetic susceptibility $\Delta\chi$ of the phospholipids, resulting in a preferred orientation of the molecules in the magnetic field. Nevertheless, magnetic orientability is still in competition with thermal fluctuations and might be difficult to detect. The magnetic orientation of the bilayer can be increased significantly with the chemical complexation of lanthanide ions to the

phospholipids. The direction of the alignment depends on the lanthanide ion used. Thulium (Tm^{3+}) will result in a parallel aligning, and Dysprosium (Dy^{3+}) in a perpendicular aligning of the bicellar normal to the magnetic field [7, 8]. Such an enhancement of the magnetic susceptibility anisotropy will result in a pronounced magnetic alignment of the bicelles subjected to an external magnetic field [9-12]. Figure 2 shows a schematic representation of the orientation of lanthanide doped bicelles as well as their anisotropic small-angle neutron scattering pattern when subjected to a magnetic field. As depicted in Figure 2 the presence of complexed lanthanide in the planar sheet of the bicelle is not likely because of the unfavorable packing parameter of the doped phospholipids. Here, we mainly find

the lamellae forming phospholipids, i.e., DMPC, while DMPE-DTPA/lanthanide with its large head group is assumed to cover the highly curved end cap [9].

To improve the amount of the lanthanide/DMPE-DTPA complex in the lamellar part of the bicelles, cholesterol was introduced into the mixture. Due to its bulky hydrophobic part, cholesterol increases the lateral distance of the headgroups in the bilayer, thus allowing a larger fraction of the chelator-lipid into the plane of the disk, thereby increasing the disk size and the magnetic alignability [10]. In a second step we were able to directly chelate lanthanides to cholesterol and thus anchor Thulium or Dysprosium in the planar region of the bicelle. Figure 3 shows schematically the inclusion of cholesterol molecules and

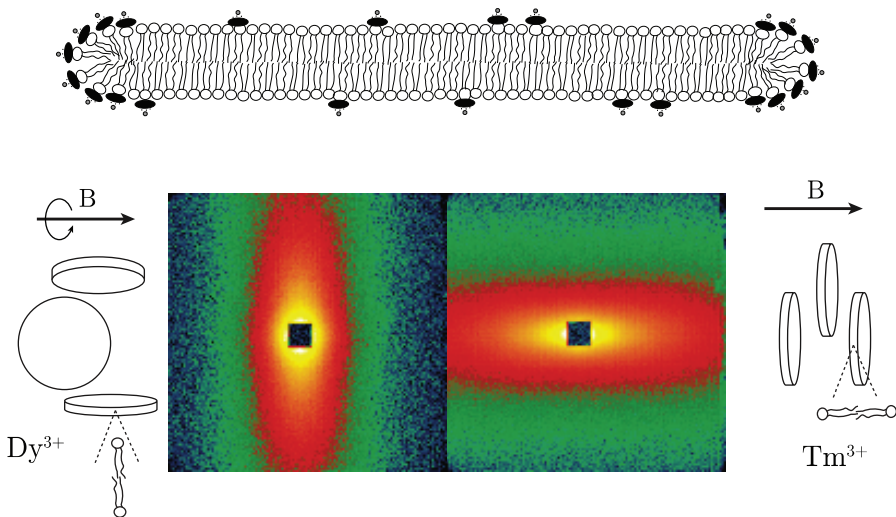


Figure 2: Depending on the diamagnetic susceptibility $\Delta\chi$ of the lanthanides the bicellar normal will either orientate perpendicular (Dy^{3+}) or parallel (Tm^{3+}) to the magnetic field (bottom, adapted from Liebi [12]). The 2D-SANS patterns show the anisotropic orientation of the aqueous bicellar solution.

cholesterol-anchored lanthanides in the lamellae sheet and the resulting SANS pattern of the magnetically oriented material [11].

Bicelles undergo structural changes with temperature, which are related to the phase transition temperature T_m of the phospholipids. Disk-shaped aggregates with the most pronounced aligning properties have been found at temperatures below T_m [10]. In order to optimize the degree of alignment in the gelatin-bicelles system, T_m of the phospholip-

ids should preferentially lie above the gelation temperature of gelatin. Hence, the fatty acid tail myristoyl was replaced by palmitoyl in the bicellar mixture shifting the phase transition temperature of 23.6°C away from the melting temperature of gelatin, which is in the order of 22 – 32°C, to a phase transition temperature of 41.3°C [13].

Cryo-TEM micrographs of an aqueous mixture of DPPC/Chol/DPPE-DTPA/Tm³⁺ show the presence of bicelles and a few vesicles as

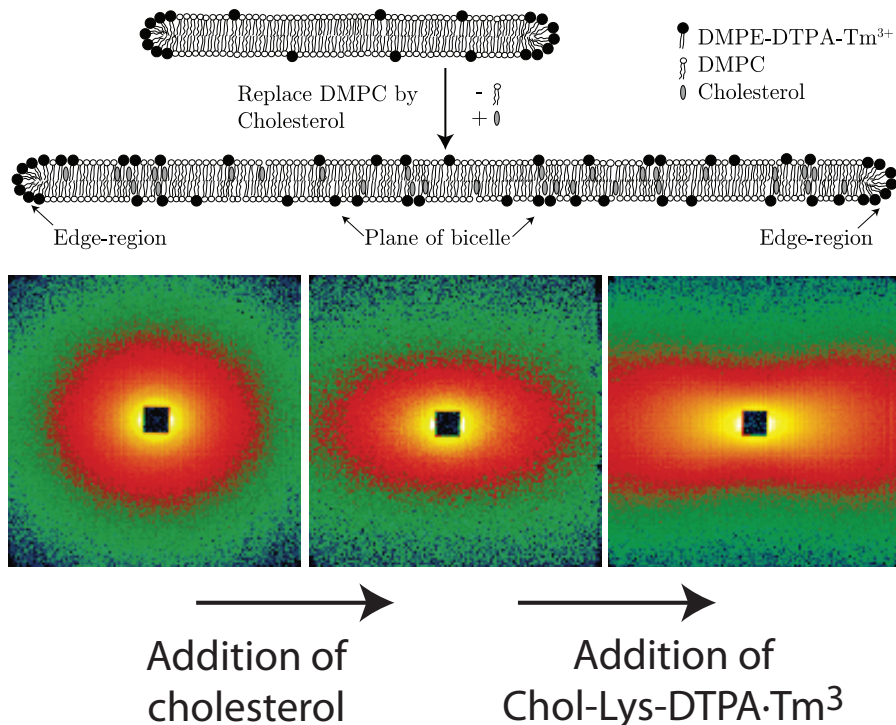


Figure 3: Addition of cholesterol and cholesterol-anchored lanthanides lead to an increase of bicelle size and an increased number of lanthanides present in the lamellae sheet (top, adapted from Liebi [13]). The 2D-SANS patterns show the anisotropic orientation of the original bicelles (bottom left) with added cholesterol (bottom middle) and with cholesterol-anchored Thulium (bottom right). The increasing alignability in the magnetic field can clearly be observed.

depicted in Figure 4. The flat structure of the bicellar aggregates was verified by taking cryo-TEM images at different tilt angles showing the same bicelle face-on (Figure 4A) and in a partial edge-on view (Figure 4B) in analogy to what had been found previously for DMPC/Chol/DMPE-DTPA/Tm³⁺ bicelles [10, 14].

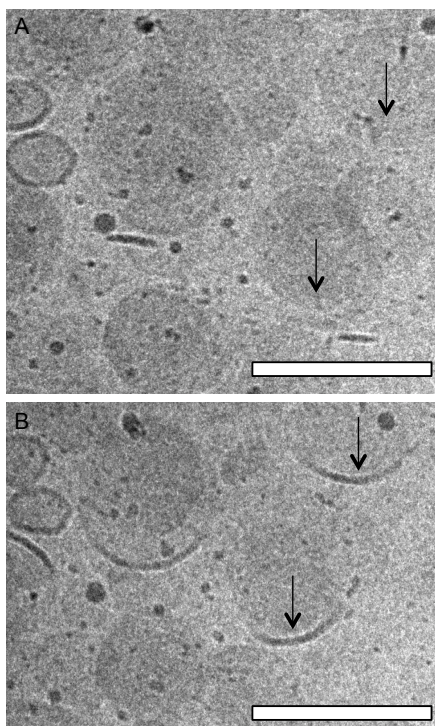


Figure 4: Cryo-TEM micrographs of an aqueous mixture of DPPC/Chol/DPPE-DTPA/Tm³⁺ showing bicelles and a few vesicles. To confirm the disk-like shape of the bicelles two images with different tilt angles were taken (0° for image A and 30° for image B). Arrows point to bicelles, which are in face-on view (A) and getting into edge-on view at the lower border (B). The scale bar represents 200 nm (image adapted from Liebi [14]).

All previously discussed steps, i.e. the complexation of lanthanides to phospholipids, introduction of cholesterol and cholesterol-anchored lanthanides, as well as the modification of the fatty acids focus on the design and optimization of a magnetically switchable structure, which can be locked reversibly by lowering the temperature. Therefore it is crucial that the final hydrogel retains the properties of both the bicelles, i.e. structural integrity and alignability, and of the gel, i.e. gel forming properties, as discussed in the next section.

TOWARDS SMART HYDROGELS: BICELLES IN GELATIN

Gelatin powder was added to the bicellar solution and mixed at 50°C, i.e. above the melting point of gelatin. Gelatin was chosen because of its thermo-reversible gelation behavior. Several studies of phospholipid vesicles in gelatin, collagen, or cross-linked gelatin matrices indicate the ability of these biopolymer gels to entrap phospholipid aggregates without destroying them [15-17]. Other gel-forming biopolymers such as pectin, κ-carrageenan, or alginate are charged systems and therefore could interfere or even destroy the bicellar morphology. In Figure 5 SANS intensity curves show the influence of gelatin on the structure of the bicelles without applied magnetic field. The radially averaged curves of DPPC/Chol/DPPE-DTPA/Tm³⁺ without gelatin and embedded into 5% (w/w) gelatin at 40°C and 0 T are shown together with the scattering curve for pure gelatin solution [14].

The scattering intensity of bicellar solutions (with or without gelatin) dominates over that from gelatin alone allow evidently a good distinction between gel phase and embedded bicelles. To elucidate if gelatin interferes with the bicellar morphology, DPPC/Chol/DPPE-DTPA/Tm³⁺ bicelles without gelatin are fitted with a form factor for flat cylinders resulting in a thickness of 4.9 nm and a radius of 80.2 nm. The thickness is in good agreement with literature values on DPPC bilayers containing cholesterol [18]. The fit of the bicelles embedded into the gelatin system result in the same form factor and dimensions but includes an additional structure factor for multilamellar structures accounting for a stacking of the bicelles (for details see Liebi [14]).

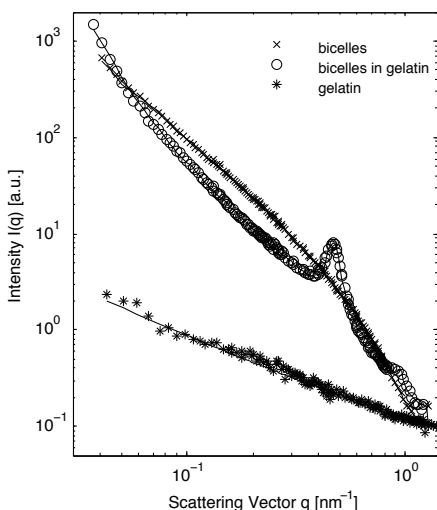


Figure 5: Radially averaged SANS curves and corresponding fit of DPPC/Chol/DPPE-DTPA/Tm³⁺ bicelles with and without 5 % (w/w) gelatin and of gelatin only. Temperature was 40°C and no magnetic field was applied, adapted from Liebi [14].

The distinct peak found for bicelles embedded into the gelatin system is explained by stacking of the bicelles. The stacking is most probably caused by thermodynamically driven depletion interaction between the particulated aggregates, i.e. bicelles, and the polymer molecules, i.e. gelatin. As a result of depletion, clustering of the bicelles and microscopic phase separation leads presumably to the stacking of the bicelles, which can also be seen as localized nematic arrangements embedded in gelatin as depicted in Figure 9. Nevertheless, it can be concluded that the addition of gelatin does not alter the morphology of the individual bicelles but initiates a stacking mechanism most probably due to depletion [14].

SANS measurements of the same samples cooled from 40°C to 5°C in the presence of an 8 T field were conducted inside a magnet. In Figure 6A and 6B, 2D-SANS patterns of DPPC/Chol/DPPE-DTPA/Tm³⁺ with and without gelatin are depicted. The anisotropy of the scattering pattern indicates the alignment of the bicelles in the magnetic field with their disk normal parallel to the magnetic field direction. The anisotropy of the bicelles embedded into the gelled gelatin (Figure 6B) is more pronounced than for pure non-gelled bicellar solution (Figure 6A) due to stacking. The stacking results in an increasing of the aggregation number, which is proportional to the magnetic orientation energy [19]. The distinct peak in the direction of the magnetic field corresponds to the stacking distance, which is slightly shifted with temperature from 13.2 nm at 40°C to 14.4 nm at 5°C. Keeping the temperature at 5°C but removing the

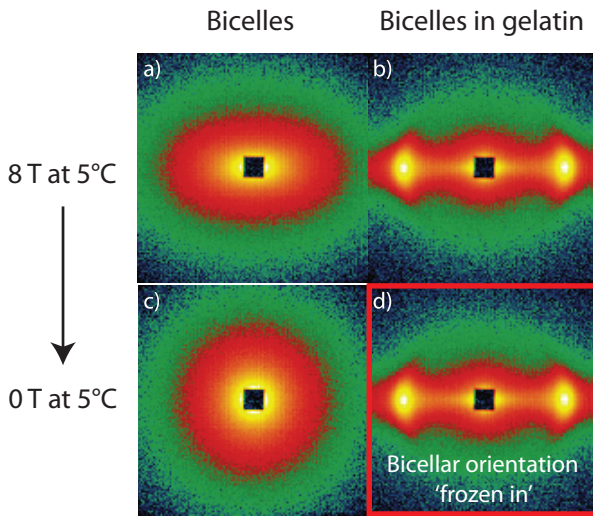


Figure 6: 2D SANS pattern of DPPC/Chol/DPPE-DTPA/Tm³⁺ bicelles without (A, C) and with (B, D) gelatin measured at 5°C. Images A and B are measured at 8 T while images C and D were taken after the magnet was ramped down to 0 T. Magnetic field direction is horizontal in the plane (adapted from Liebi [14]).

magnetic field results in 2D-SANS patterns as shown in Figure 6C and 6D. Whereas the pure non-gelled bicellar solution relaxes back to an isotropic scattering with no preferential orientation (Figure 6C), the bicelles embedded in gelled gelatin keep their orientation even after removal of the magnetic field (Figure 6D) [14].

The temperature dependence of the bicellar alignment with and without gelatin is shown in Figure 7 utilizing the anisotropy factor A_f calculated from 2D SANS pattern [10]. If the pure bicelle solution is cooled at 8 T, the alignment factor decreases slightly, indicating a pronounced orientation with decreasing temperature (star symbols in Figure 7). If the bicelles are embedded into the gelatin system, A_f decreases with decreasing temperature from 40°C to 20°C but is constant if the temperature is lowered further (solid circles in Figure 7). This coincides with

the gelation point of gelatin, which is around 22°C for this cooling rate as determined with rheological measurements. If the sample is heated after switching off the magnetic field (open circles in Figure 7), the alignment remains fairly constant until about 30°C, i.e. the melting point of gelatin, where the bicelles start to randomize their orientation until the alignment factor reaches 0 (isotropic scattering pattern) [14].

In order to read the bicellar orientation in the gel, with regard to a possible application of such bicelle containing macrostructure as a smart material, we studied its anisotropy for electromagnetic wave transmission. Therefore, birefringence measurements were carried out on DPPC/Chol/DPPE-DTPA complexed with either Thulium or Dysprosium, which are gelled inside a magnetic field and measured after removal of the field in all three spatial directions (see Figure 8). The optical anisot-

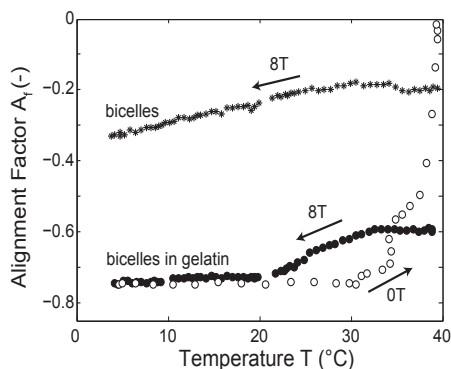


Figure 7: Alignment factor A_f as a function of temperature of bicelles with and without gelatin. Pure bicellar solution shows a moderate decrease of A_f with decreasing temperature (star symbols). With gelatin present and the magnetic field switched on, the A_f is already much lower and further decreases until the gelling temperature of 22°C is reached and no further alignment and orientation is possible (solid circles). The heating cycle was performed without magnetic field applied and result in a complete loss of orientation once the melting temperature of gelatin at 32°C is reached (open circles) (adapted from Liebi [14]).

ropy results from both the molecular composition, i.e. intrinsic birefringence and the self-assembled mesostructure, i.e. form birefringence [20]. In our case the optical axis of the phospholipid molecules is parallel to its fatty acid tails and no birefringence is observed if measured in the direction of the long molecular axis. This is the case of bicelles with complexed Thulium measured in the direction of the z-axis (Figure 8, face-on view of bicelles, indicated with white circles). If the birefringence is measured in the direction of the y-axis, the molecules doped with Thulium show a positive birefringence value (bicelles in edge-on view, green disks). Molecules with Dysprosium aligning with their long-molecular axis perpendicular to the magnetic field can still rotate around the magnetic field axis. As a consequence, they will be oriented either in the direction of the x-axis, showing a negative birefringence value (bicelles in edge-on view, red disks), or in the direction of y-axis, thus

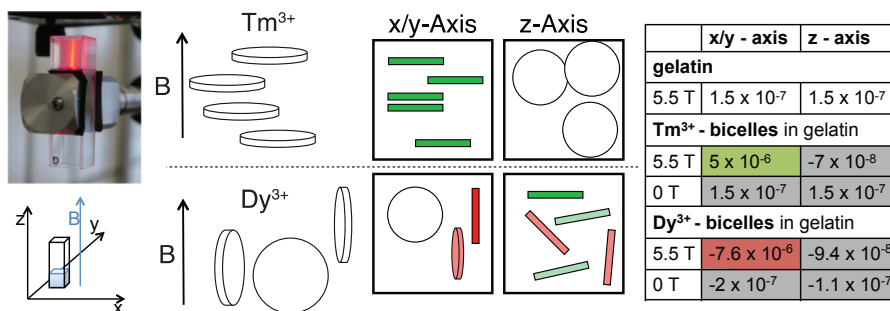


Figure 8: Measuring a gel cube for spatial differences of birefringence (top left). Schematic representation of the bicellar orientation in the magnetic field. Shading indicates the birefringence signal measured in the different spatial orientations, with green for positive, red for negative birefringence, and white for no birefringence (middle). The actual measured birefringence values are summarized in the table (adapted from Liebi [14]).

showing no birefringence (bicelles in face-on view, white) if measured in the x/y -plane. Measured in the z -axis, Dysprosium bicelles are found face-on in all possible directions and the overall birefringence signal is canceled out [14]. No significant change of the birefringence signal compared to the background was observed for the control, which was gelled without applied magnetic field. The measured values of the birefringence are summarized as a table in Figure 8.

CONCLUSION

We present magnetic alignable bicelles embedded in a gelatin matrix generating magnetically switchable structures, which can reversibly be locked and unlocked by adjusting the temperature. As shown with SANS meas-

urements, the alignment stays unchanged after removal of the magnetic field until up to about 30°C , which is the melting point of gelatin. Stacking of the bicelles induced by the gelatin promotes magnetic alignment, as an increased aggregation number in the stacks increases the magnetic orientation energy. The resulting gel cubes show different spatial birefringence. Cycling through the melting point of gelatin sets the structure back to its isotropic state providing a readout of the thermal history. Thus, it can be used as sensor e.g. reporting unwanted thawing-cooling cycles of sensitive goods. All results are in agreement with a successful fixation of the magnetic field orientation of the bicelles by gelatin as summarized in Figure 9.

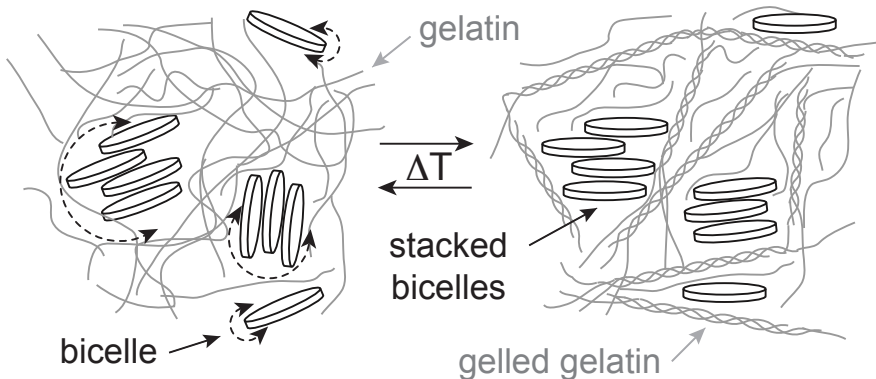


Figure 9: Schematic representation of the bicellar arrangement and orientation in gelatin matrix. Above the melting temperature and with no magnetic field applied, random orientation of the bicelles and bicellar stacks is observed (left) leading to an isotropic birefringence signal. Cooling and gelation in presence of a magnetic field orients and fixes the bicellar structures leading to an anisotropic alignment and, thus, a birefringence signal can be detected (right). Adapted from Liebi [14].

ACKNOWLEDGMENT

This contribution summarizes already published manuscripts where detailed information on bicelle preparation, chemical modifications, experimental methods, and data treat-

ment can be found [10-12, 14]. The work is based on experiments performed at the Swiss Spallation Neutron Source SINQ, Paul Scherrer Institute, Villigen, Switzerland. The Swiss National Foundation is acknowledged for funding (Project number 200021_132132).

REFERENCES

- [1] Gil, E. S.; Hudson, S. M. *Prog. Polym. Sci.* 2004, 29, 1173 – 1222
- [2] Kumar, A.; Srivastava, A.; Galaev, I. Y.; Mattiasson, B. *Prog. Polym. Sci.* 2007, 32, 1205– 1237
- [3] Satarkar, N. S.; Biswal, D.; Hilt, J. Z. *Soft Matter* 2010, 6, 2364 – 2371
- [4] Liu, T.-Y.; Hu, S.-H.; Liu, D.-M.; Chen, S.-Y.; Chen, I. W. *Nano Today* 2009, 4, 52 – 65
- [5] Liu, T.-Y.; Hu, S.-H.; Liu, K.-H.; Liu, D.-M.; Chen, S.-Y. *J. Controlled Release* 2008, 126, 228 – 236
- [6] Zrinyi, M. *Colloid Polym. Sci.* 2000, 278, 98 – 103
- [7] Binnemans, K.; Gorller-Walrand, C. *Chem. Rev.* 2002, 102, 2303 – 2345
- [8] Prosser, R. S.; Volkov, V. B.; Shiyonovskaya, I. V. *Biophys. J.* 1998, 75, 2163 – 2169
- [9] Beck, P.; Liebi, M.; Kohlbrecher, J.; Ishikawa, T.; Rüegger, H.; Fischer, P.; Walde, P.; Windhab, E. J. *Langmuir* 2010, 26, 5382 – 5387
- [10] Liebi, M.; Kohlbrecher, J.; Ishikawa, T.; Fischer, P.; Walde, P.; Windhab, E. J. *Langmuir* 2012, 28, 10905 – 10915
- [11] Liebi, M.; Kuster, S.; Kohlbrecher, J.; Ishikawa, T.; Fischer, P.; Walde, P.; Windhab, E. J. *J. Phys. Chem. B* 2013, 117, 14743 – 14748
- [12] Liebi, M.; van Rhee, P. G.; Christianen, P. C. M.; Kohlbrecher, J.; Fischer, P.; Walde, P.; Windhab, E. J. *Langmuir* 2013, 29, 3467 – 3473
- [13] Koynova, R.; Caffrey, M. *Biochim. Biophys. Acta* 1998, 1376, 91 – 145
- [14] Liebi, M.; Kuster, S.; Kohlbrecher, J.; Ishikawa, T.; Fischer, P.; Walde, P.; Windhab, E. J. *ACS Applied Materials & Interfaces* 2014, 6, 1100 – 1105
- [15] DiTizio, V.; Ferguson, G. W.; Mittelman, M. W.; Khoury, A. E.; Bruce, A. W.; DiCosmo, F. *Biomaterials* 1998, 19, 1877 – 1884
- [16] Dowling, M. B.; Lee, J.-H.; Raghavan, S. R. *Langmuir* 2009, 25, 8519 – 8525
- [17] Weiner, A. L.; Carpenter-Green, S. S.; Soehngen, E. C.; Lenk, R. P.; Popescu, M. C. *J. Pharm. Sci.* 1985, 74, 922 – 925
- [18] Reinl, H.; Brumm, T.; Bayerl, T. M. *Biophys. J.* 1992, 61, 1025 – 1035
- [19] Qiu, X. X.; Mirau, P. A.; Pidgeon, C. *Biochim. Biophys. Acta* 1993, 1147, 59 – 72
- [20] Lee, C. W.; Decca, R. S.; Wassall, S. R.; Breen, J. J. *Phys. Rev. E* 2003, 67, 061914

Elucidating the biography of a proton in a proton conductor with neutrons and X-rays

Qianli Chen^{1,2,a}, Artur Braun¹

¹Laboratory for High Performance Ceramics
Empa - Swiss Federal Laboratories for Materials Science and Technology
CH-8600 Dübendorf, Switzerland

²Department of Physics, ETH Zürich
CH-8057 Zürich, Switzerland

^aCurrent address:
Max Planck Institute for Polymer Research
Ackermannweg 10
D-55128 Mainz, Germany

PROTONS IN HYDROGEN ECONOMY

Protons and hydrogen, when incorporated in solid matter, can have significant influence on the properties of the materials. Materials relevant for a hydrogen economy, a term first mentioned half a century ago,[1] should thus be compatible with hydrogen and protons. An important example dates back actually one full century ago and played an important role for the industrial scale Ammoniaksynthese by Haber and Bosch.[2] Given its huge impact on the development of global population by its use of hydrogen, it is not far-fetched to

consider the Haber Bosch process as the beginning of the hydrogen economy. Specifically, the Haber Bosch process requires reaction vessels which can sustain high pressure at high temperatures. The hydrogen involved in the Ammoniaksynthese would diffuse in the vessels and react with the carbon atoms of steel and impact its toughness, resulting in dangerous explosions during synthesis: A striking example for the deleterious interaction of hydrogen with materials. In this paper we will showcase how protons can have beneficial use when they are used as charge carriers in solid fuel cell electrolytes.

One example is the ceramic proton conductor. As alternatives to conventional oxygen ion conductors, ceramic proton conductors are applied as solid electrolyte membranes in electrochemical energy converters such as ceramic fuel cells and electrolyzers. The operating temperature is typically lower than that for oxygen ion conductors, which reduces the material costs, and operating complexities. However, the proton conductivity still needs to be improved before these materials are used in commercial devices. To control the performance of the proton conducting electrolytes, it is essential to understand the proton conduction mechanism at the molecular scale.

We studied one of the contemporary ceramic proton conductors with high proton conductivity – yttrium-substituted barium cerate ($\text{BaCe}_{1-x}\text{Y}_x\text{O}_{3-\delta}$, BCY). This material has the

ABO_3 -type perovskite structure with Ba atoms on the A-site, and Ce atoms on the B-site. Each Ce is surrounded by 6 oxygen ions forming an octahedron. Substitution of Ce^{4+} by Y^{3+} creates oxygen vacancies which are filled by surrounding water molecules, and the protons are introduced and bond to the lattice oxygen. Fig. 1 is a schematic of the crystal structure of BCY.

HOW PROTONS DIFFUSE? THE EXISTING CONFLICTS AND ROLE OF NEUTRONS

The common perception is that in perovskites, the protons diffuse by hopping from one oxygen site to another, known as the Grotthuss mechanism [3-6], which includes the rotation of proton around the oxygen, and the subsequent jump of a proton and transfer to another oxygen site (blue arrows in Fig. 1). The energy barrier

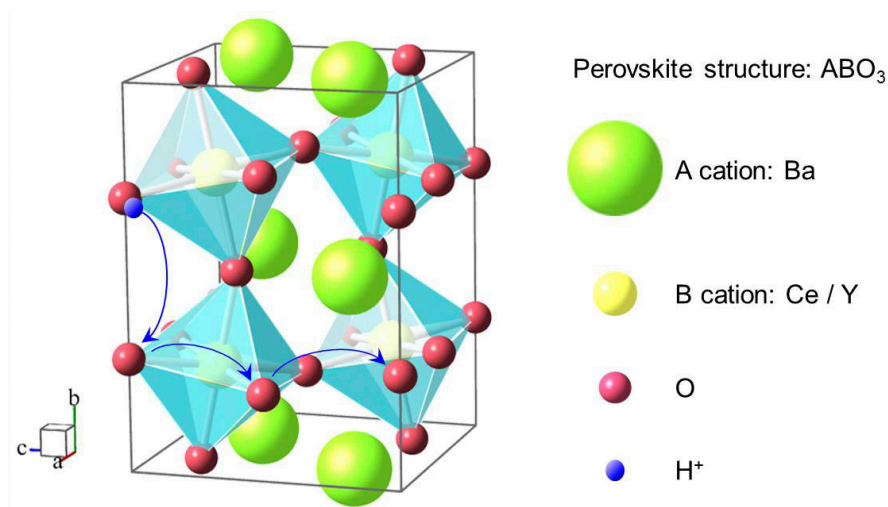


Fig. 1: A proton in a representative proton conducting perovskite material $\text{BaCe}_{1-x}\text{Y}_x\text{O}_{3-\delta}$. Blue arrows indicate possible traces for proton jump from one oxygen site to another.

in the jump process dominates the energy needed in the proton hopping.

Better proton conductivity requires lowering this energy barrier.

In the Grotthuss mechanism, when the oxygen distance is smaller, this energy barrier should be lower [7]. However, in earlier works at Empa it was observed that the activation energy is smaller when the lattice parameter of the material is larger.[8] A dependency of activation energy from the lattice volume is found not only when tuning the lattice chemical approaches, such as changing the synthesis routes and temperatures,[8] but also by a more direct and straightforward application of external mechanical strain. Our initial impedance spectroscopy studies at high pressure and high temperatures [9, 10] (with the facilities and assistance from Nickolai Bagdasarov, Goethe University Frankfurt) provide solid proof that the activation barrier increases with the applied pressure, see Fig. 2 (we have converted the pressure into elastic

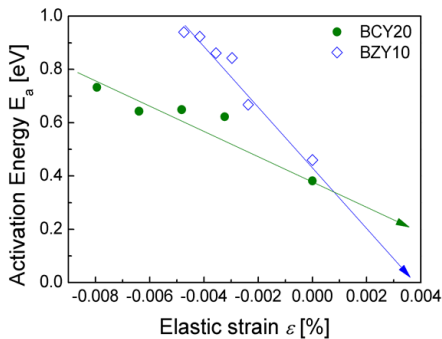


Fig. 2: Variation of activation energy of bulk conductivity on the on the elastic strain parameter ϵ for $\text{BaCe}_{0.8}\text{Y}_{0.2}\text{O}_{3-\delta}$ (BCY20) and $\text{BaZr}_{0.9}\text{Y}_{0.1}\text{O}_{3-\delta}$ (BZY10). BCY20 data are taken from Ref. [10] and BZY10 data are from Ref. [9].

strain). Therefore we were confident that there was not any chemical effect behind the changed activation energy, but a relatively simple physical process. More space in the lattice would make protons easy to move.

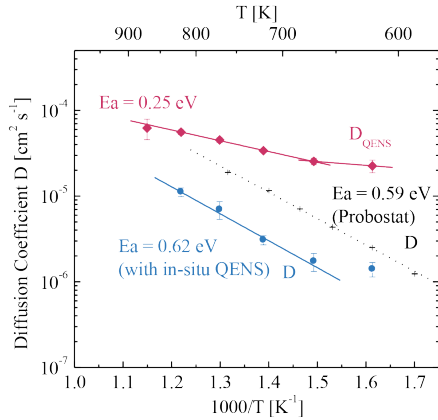


Fig. 3: Arrhenius plot of the self-diffusion coefficient D_{QENS} for $\text{BaCe}_{0.8}\text{Y}_{0.2}\text{O}_{3-\delta}$ measured by QENS, and the bulk conductivity diffusion coefficient D_0 taken in-situ by EIS (dotted line: another reference sample measured individually in Probatat at $p(\text{H}_2\text{O}) = 2200$ Pa).

This hypothesis on the lattice volume versus activation energy still needed to be tested and verified. Impedance spectroscopy is a well-established method for studying the charge carrier dynamics in fuel cell components. It does however not discriminate between electrons, protons and other ions. On the other hand, neutron methods should always be considered when hydrogen or protons are key players in a system. As we will see, we used quasi elastic neutron scattering (QENS) for the determination of the proton dynamics. Fig. 3 shows the diffusion coeffi-

cients for proton diffusion as obtained from impedance spectroscopy and QENS for temperatures from 600 K to 900 K. With respect to tackling materials issues for a hydrogen economy, neutrons appear generally a preferred choice as probes for hydrogen and protons.

TOWARDS HIGH PRESSURE

From the application point of view, for solid electrolyte membranes, it is desirable to have materials with lower activation energy for protons, and therefore larger lattice parameters. But technically it is almost impossible to enlarge, to expand a crystal lattice unless one considers epitaxial strained films. Epitaxial film proton conductors may indeed be the future solution for superprotonic membrane technology in solid oxide fuel cells. However, studying the proton dynamics of an ultrathin epitaxial film with quasi elastic neutron scattering is not viable in view of the very small amounts of material that come with ultrathin films, in contrast to large amounts of material necessary for QENS. We therefore chose a pragmatic solution, this is, applying compressive strain on proton conductor monolith samples. The stress-strain-

activation barrier relationship should be the same for strained epitaxial films and for compressed monoliths.

There are a lot of readily existing pressure apparatuses used for different techniques. In order to gain a complete overview for the correlation of the material structure and properties, we have employed a piston-cylinder clamp cell for impedance spectroscopy as mentioned before, diamond anvil cells for high pressure X-ray diffraction (facilities from Simon M Clark, California High Pressure Observatory and Advanced Light Source)[11] and high pressure Raman spectroscopy (facilities from Wendy Mao, Stanford University).[11] Nevertheless, measuring with neutrons under pressure turned out to be a challenge that we had to solve pragmatically.

To study proton diffusion by neutron scattering at high pressure and high temperature, a new cell was designed and built at Empa[12] (Fig. 4) in collaboration with Stuart Holdsworth, and many scientific suggestions came from Thierry Strässle and Jan Embs (PSI). We employed a simple piston-cylinder cell design. The cell is developed with the requirement to impose and maintain 1 GPa pressure at temperatures up to 770 K. It is in this case a pure coincidence that progress in a hydrogen



Fig. 4: Empa high pressure neutron cell (the position of the sample powder inside is marked as shadow).

economy relevant research project requires advancement in materials technology, as here with the availability of a high quality INCONEL® alloy. This cell has been tested for neutron diffraction, and for inelastic and quasi-elastic neutron scattering at various temperatures and pressures. With this cell we managed the first high (p,T) inelastic and quasielastic neutron scattering experiment to our knowledge.

Our first challenge is the design of the high pressure cell for neutron scattering, since several requirements are necessary to be fulfilled:

- (1) Large enough sample volume is required for the current flux rates of neutron sources require to obtain acceptable signal-to-noise ratio in reasonable time;
- (2) The mechanical and thermal properties of the cell should allow it to operate at the required temperature and pressure;
- (3) In order to use the available neutron scattering facilities at SINQ and ILL, without significant equipment resource investment, it was also necessary to design and construct a cell which could be pressurized remotely before introduction into the readily existing furnace facility at the beam line to be used. In so far the readily existing infrastructure at the neutron facilities posed prior constraints on the external dimensions of the high pressure neutron cell.
- (4) The cell should have no unwanted scattering and absorption caused by the cell body in the neutron beam path.

According to these requirements we optimized the dimension of the cell. We chose

Nickel-based INCONEL® alloy 718 as cell wall material.

The pressure inside the cell is measured by reading the strain gauges attached to the outer cell wall when loading the pressure. Since the pressure is related to the change of the lattice volume by the equation of state, we were able to confirm the pressure by neutron diffraction at HRPT, SINQ (Fig. 5) with Vladimir Pomjakushin.

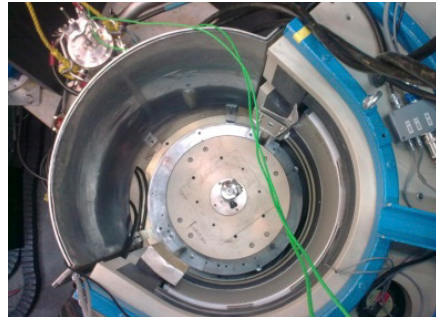


Fig. 5: Empa high pressure cell in HRPT at SINQ

PROBING THE PROTON DYNAMICS WITH NEUTRONS UNDER HIGH PRESSURE

Inelastic neutron scattering provides insight in the lattice dynamics of condensed matter. We performed inelastic neutron scattering at high temperatures in our pressure cell at the cold neutron backscattering spectrometer IN16, Institut Laue-Langevin, Grenoble (with the support from Bernhard Frick), see Fig.4. We found that at high pressure, shift of the step in the elastic scattered intensity decrease to higher temperature, which is an indication of the slow down of the proton dynamics.[12]



Fig. 6: At IN16, ILL. Tzu-Wen Huang (Empa) and Bernhard Frick were mounting the Empa high pressure cell in the spectrometer.

QENS is a good tool to study hydrogen diffusion because hydrogen has a much larger incoherent scattering cross section than other elements. We studied the proton diffusion process by QENS at the time-of-flight spectrometer FOCUS, SINQ (with the support from Jan Embs). At ambient pressure, the quasielastic function gets broader with the increasing of temperature, indicating increasing proton diffusivity. From QENS we are able to derive the proton diffusion coefficient, average proton jumping length and jump rate. [13, 14]

QENS under high pressure at high temperature posed a challenge. The difficulty in this measurement is that the neutrons have to pass through the thick 5mm cell wall for two times (whereas the inner diameter of the cell is also 5mm). Therefore it is challenging to resolve the quasielastic signal from the protons apart from the pressure cell, as only

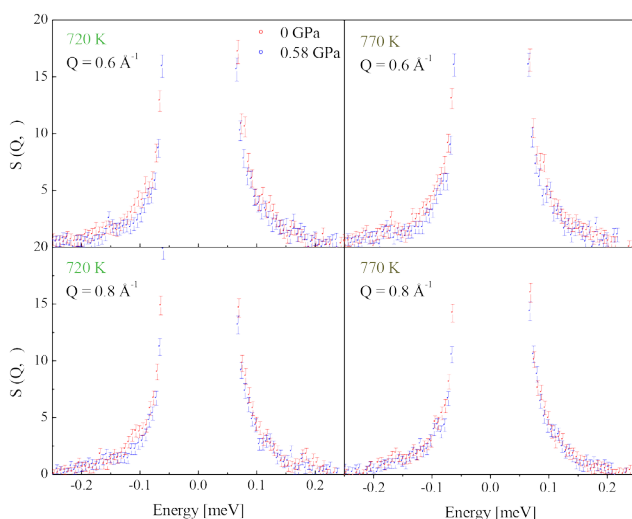


Fig. 7: Comparison of time-of-flight QENS spectra from protonated BCY20, without and with pressure ($p = 0.58$ GPa) at 720 K and 770 K, all recorded in the HTP-cell with $Q = 0.6 \text{ \AA}^{-1}$ and 0.8 \AA^{-1} (the original figure is in colour).

a small portion of neutrons detected are contributed by the materials inside the cell. We managed QENS measurement for the first time up at 770K at 0.83 GPa at FOCUS, SINQ. Fortunately, as is obvious from Fig. 7, we were able to resolve that the spectrum without pressure is broader than the one with pressure, meaning that at higher pressure, there is reduced diffusion of hydrogen.[12]

CHEMISTRY – THE OTHER PART OF THE MULTI-EXPERIMENT PIZZA

Although energy converter materials may look simple from the outside, they are actually more complicated inside. A handful of questions needed to be addressed with more than one method. This reflects both the physics

and the chemistry. The neutrons deliver us dynamics information but not the chemistry, therefore we turned to synchrotron X-ray.

A water molecule, being added as part into a crystal lattice - this is where engineered vacancies play an important role. The protons are structural elements in water, and then become structural elements in a crystal lattice of proton conductors.[15] Then at high temperatures, protons get shaken up with the phonons and couple to something which is reminiscent of a polaron.[†] Eventually, the chemical bonds brake at certain temperature. We monitored the formation and breaking of bonds with ambient pressure X-ray photoelectron spectroscopy at Beamline 9.3.2 at the Advanced Light Source in Berkeley, California (with the support from Zhi Liu, ALS and Farid El Gabaly, Sandia National Laboratories).

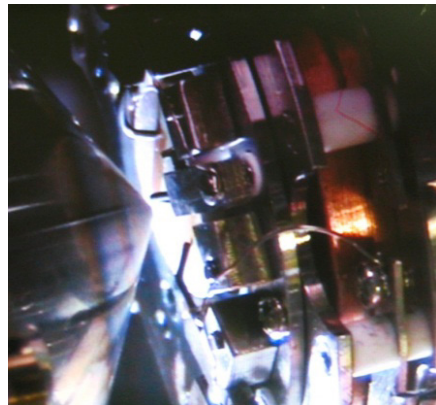
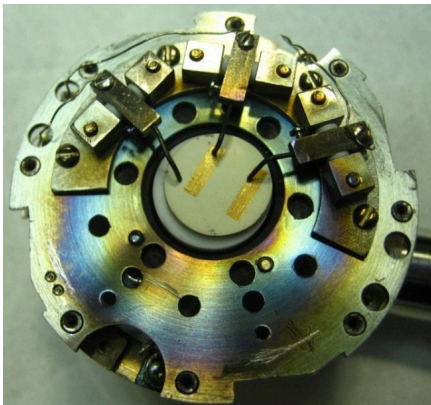


Fig. 8: proton conductor sample pellet sputtered with gold electrodes, mounted on the sample holder (left) and when it is in the XPS beam (right).

[†] This still under controversial debate.

Figure 9 compares the Ce4p resonant photoemission valence band spectra of BCY20 under dry UHV and wet (150 mTorr water vapor partial pressure) condition. We can identify very easily the spectral signatures of

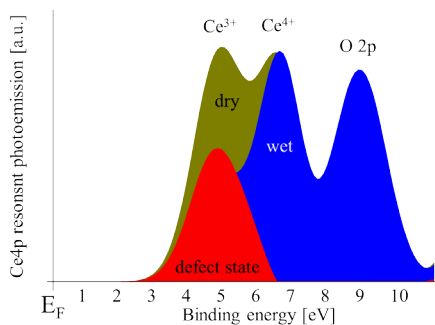


Fig. 9: X-ray photoemission valence band spectra of BCY20 recorded under Ce4p resonant x-ray energy for dry (UHV) and wet conditions (150 mTorr water vapor pressure). The defect state is formed by oxygen vacancies and disappears upon exposure to water vapor pressure.

Ce³⁺ and Ce⁴⁺ species before the O2p oxygen bonding peak at around 5eV, 7eV, and 9eV, respectively. The dry sample contains oxygen vacancies which give rise to a defect state in the valence band. Upon exposure to water vapor, this defect state gets diminished.

Our resonant photoemission studies of dry and wet proton conductor samples show that oxygen ligand holes in the proximity of the Y dopant (which forces the oxygen vacancies into the lattice) are by around 0.5 eV closer to the Fermi level than the corresponding hole states from Ce, see Figure 10.

We observed the filling of oxygen vacancy in proton conductors under water vapor. We could see three different temperature regimes for the proton transport along with the structural change of BCY: at ambient T (structural protons), at moderately annealed T (proton-polarons), and at high T (breaking of bonds). From in-situ electrochemical impedance

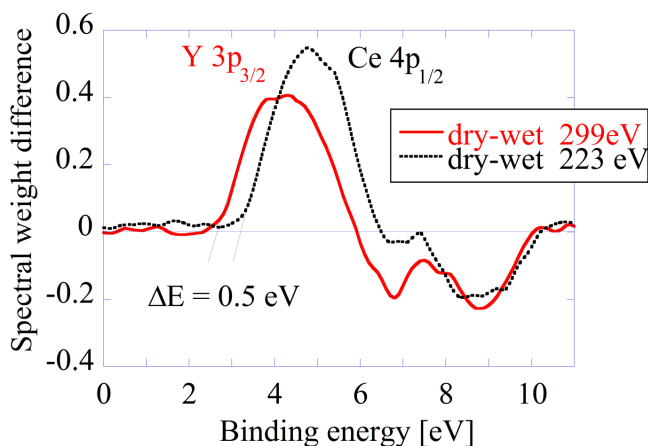


Fig. 10: Comparison of the valence band difference spectra (spectrum under dry condition minus spectrum under wet condition) recorded in Y3p and Ce4p resonant X-ray energies (299eV and 223eV, respectively). Note the shift of the valence band maximum of 0.5 eV towards EF for the Y-resonant spectrum.

spectroscopy we measured the corresponding increase in electric conductivity is paralleled by chemical shifts in the oxygen core level spectra.[16]

A LOOK TO THE FUTURE

Knowing the relation of the activation energy versus the elastic strain, it becomes clear that we have to expand the lattice with

tensile strain, to get higher proton mobility. One can do this with epitaxial films. This may provide a general guideline for epitaxial strained proton conducting thin film systems with high proton mobility and low activation energy. We would be interested to investigate the strained epitaxial proton conductors, but unfortunately, QENS is not possible of thin film samples. We look forward to progresses in the neutron optics and detectors, so that QENS on thin films become possible.

REFERENCES

- [1] J. O. M. Bockris, *International Journal of Hydrogen Energy* **38** (6), 2579-2588 (2013).
- [2] J. W. Erisman, M. A. Sutton, J. Galloway, Z. Klimont and W. Winiwarter, *Nature Geoscience* **1** (10), 636-639 (2008).
- [3] S. Cukierman, *Biochimica et Biophysica Acta (BBA) - Bioenergetics* **1757** (8), 876-885 (2006).
- [4] R. Hempelmann, C. Karmonik, T. Matzke, M. Capadonia, U. Stimming, T. Springer and M. A. Adams, *Solid State Ionics* **77**, 152-156 (1995).
- [5] T. Norby, M. Widerøe, R. Glöckner and L. Yngve, *Dalton Trans.* **19**, 3012-3018 (2004).
- [6] M. S. Islam, R. A. Davies and J. D. Gale, *Chem. Commun.* (7), 661-662 (2001).
- [7] D. Marx, *ChemPhysChem* **7** (9), 1848-1870 (2006).
- [8] S. Duval, *Techn. Univ. München* (2008).
- [9] Q. Chen, A. Braun, A. Ovalle, C.-D. Savaniu, T. Graule and N. Bagdassarov, *Appl. Phys. Lett.* **97** (4), 041902-041903 (2010).
- [10] Q. Chen, A. Braun, S. Yoon, N. Bagdassarov and T. Graule, *J. Eur. Ceram. Soc.* **31** (14), 2657-2661 (2011).
- [11] Q. Chen, T.-W. Huang, M. Baldini, A. Hushur, V. Pomjakushin, S. Clark, W. L. Mao, M. H. Manghnani, A. Braun and T. Graule, *J. Phys. Chem. C* **115** (48), 24021-24027 (2011).
- [12] Q. Chen, S. Holdsworth, J. Embs, V. Pomjakushin, B. Frick and A. Braun, *High Pressure Research* **32** (4), 471-481 (2012).
- [13] A. Braun, S. Duval, P. Ried, J. Embs, F. Juranyi, T. Strässle, U. Stimming, R. Hempelmann, P. Holtapfels and T. Graule, *J. Appl. Electrochem.* **39** (4), 471-475 (2009).
- [14] Q. Chen, J. Banyte, X. Zhang, J. P. Embs and A. Braun, *Solid State Ionics* **252** (0), 2-6 (2013).
- [15] A. Braun, A. Ovalle, V. Pomjakushin, A. Cervellino, S. Erat, W. C. Stolte and T. Graule, *Appl. Phys. Lett.* **95** (22), 224103 (2009).
- [16] Q. Chen, F. El Gabaly, F. Aksoy Akgul, Z. Liu, B. S. Mun, S. Yamaguchi and A. Braun, *Chemistry of Materials* **25** (23), 4690-4696 (2013).

Interplay of unconventional superconductivity and magnetism in the Q-phase of CeCoIn₅

S. Gerber,^{1,2,*} M. Bartkowiak,³ J. L. Gavilano,¹ E. Ressouche,⁴ N. Egetenmeyer,¹ C. Niedermayer,¹ A. D. Bianchi,⁵ R. Movshovich,⁶ E. D. Bauer,⁶ J. D. Thompson,⁶ and M. Kenzelmann^{3, †}

¹ *Laboratory for Neutron Scattering and Imaging, Paul Scherrer Institut, CH-5232 Villigen, Switzerland*

² *Stanford Institute for Materials and Energy Sciences,*

SLAC National Accelerator Laboratory and Stanford University, Menlo Park, California 94025, USA

³ *Laboratory for Developments and Methods, Paul Scherrer Institut, CH-5232 Villigen, Switzerland*

⁴ *SPSMS, UMR-E CEA/UJF-Grenoble 1, INAC, F-38054 Grenoble, France*

⁵ *Département de Physique & RQMP, Université de Montréal, Montréal, Québec H3C 3J7, Canada*

⁶ *Condensed Matter and Magnet Science, Los Alamos National Laboratory, Los Alamos, New Mexico 87545, USA*

After S. Gerber *et al.*, Nature Phys. **10**, 126 (2014) and
PhD thesis No. 21344, ETH Zürich and Paul Scherrer Institut (2013).

The so-called cerium 115 heavy-fermions represent a prototypical material family to study the interdependence of quantum phases due to strong electron correlations. In particular, CeCoIn₅ has been at the focus of intense research activity and serves a model material for studies of unconventional superconductivity in the proximity of magnetism. Using high-field neutron scattering we show that field-induced incommensurate spin-density wave (SDW) order emerges in a continuous quantum phase transition in the superconducting Q-phase. Both orders then

break down simultaneously at the upper critical field, suggesting an intimate link between magnetism and the charge carriers. We find that always only one of two possible SDW domains is populated in the Q-phase, which cannot be explained by magnetic spin anisotropies. Carefully rotating the magnetic field direction allows for direct control and hypersensitive switching of the domain population. This binary switching behavior provides strong evidence that the Q-phase is governed by a linear coupling term of singlet superconductivity, incommensurate SDW

order and a spatially inhomogeneous triplet Cooper pair-density wave, forming a complex quantum state that can be sensitively manipulated via the control parameter of the respective quantum phase transition.

INTRODUCTION

Strongly correlated electron systems are quantum materials with a complex interplay among the charge, spin, orbital and lattice degrees of freedom from which novel quantum phases can emerge, such as magnetically-mediated superconductivity [1, 2]. In many material families, particularly in heavy-fermion systems, unconventional superconductivity is accompanied by the presence of strong magnetic fluctuations. Though these two phenomena are, in principle, of competing nature it is believed that spin fluctuations are crucial for the formation of Cooper pairs in heavy-fermion materials [2]. Therefore, it is paramount to improve our understanding of how magnetism and superconductivity interact to eventually unravel the microscopic mechanism that mediates magnetic superconductivity.

Coincident occurrence of magnetic and superconducting properties is often found in the vicinity of a quantum critical point (QCP), a state of matter at zero-temperature, where quantum fluctuations lead to a drastic change of the material properties [3]. These quantum fluctuations are believed to mediate charge, spin, orbital or lattice degrees of freedom, such that complex electronic ground states with coexisting or even cooperating order parameters emerge.

A prominent example for the later case is the heavy-fermion compound CeCoIn_5 with $T_c = 2.3$ K [4], the highest critical temperature of cerium-based superconductors, serving as a model material for studies of magnetic superconductivity and quantum criticality [5, 6].

The material is unique as a result of its cleanliness and experimental accessibility with temperature T , external magnetic fields H and applied pressure. CeCoIn_5 also shares many properties with the cuprate high-temperature superconductors, such as a quasi two-dimensional electronic structure [7], a $d_{x^2-y^2}$ -wave superconducting gap function [8–11] and a spin resonance in the superconducting state [12]. Therefore, CeCoIn_5 serves as a simple, well-controlled and accessible model material to study the interplay of magnetism and unconventional superconductivity. *Simple* should be understood in terms of the crystal structure, *well-controlled* in terms of the material cleanliness and *accessible* in terms of the available experimental techniques to probe the material also at extreme conditions. Here the latter relates to reaching distant regions of the superconducting phase, i.e., in the vicinity of the upper critical field H_{c2} and low temperatures close to absolute zero.

Though CeCoIn_5 is paramagnetic in the normal state, magnetism manifests two-fold in the superconducting phase: (i) a novel vortex structure occurs in the mixed state due to strong Pauli paramagnetic effects [13–15] and (ii) long-range spin-density wave (SDW) order emerges in the superconducting Q-phase close to H_{c2} [16–19]. Both aspects are believed to be related to the Pauli-limited superconductivity of CeCoIn_5 , where Cooper

pairs are broken up by a coupling of the electron spins to the applied magnetic field – and not by orbital depairing. Here we employ high-field neutron diffraction to directly probe the nature of the magnetic state in the presence of superconductivity and investigate how the two phenomena are coupled.

A MAGNETO-SUPERCONDUCTING QUANTUM CRITICAL POINT

Early after the discovery of $d_{x^2-y^2}$ -superconductivity in CeCoIn_5 [4] signatures of a second superconducting phase were found at high H

and low T , triggering vivid speculations on its nature [20–24]. However, later evidence was found that the so-called Q-phase has a field-induced magnetic origin [25], which was confirmed using neutron scattering [16–18]. The phenomenology of the Q-phase has also been subject of numerous theoretical studies and remains controversial to this day [26–31]. Commonalities of these approaches include (i) enhanced antiferromagnetic spin fluctuations as a consequence of magnetic quantum criticality, (ii) strong Pauli-paramagnetic pair-breaking and (iii) the possible emergence of a triplet superconducting component [5].

Figure 1 shows the diffracted neutron intensity at the Bragg peak position of the

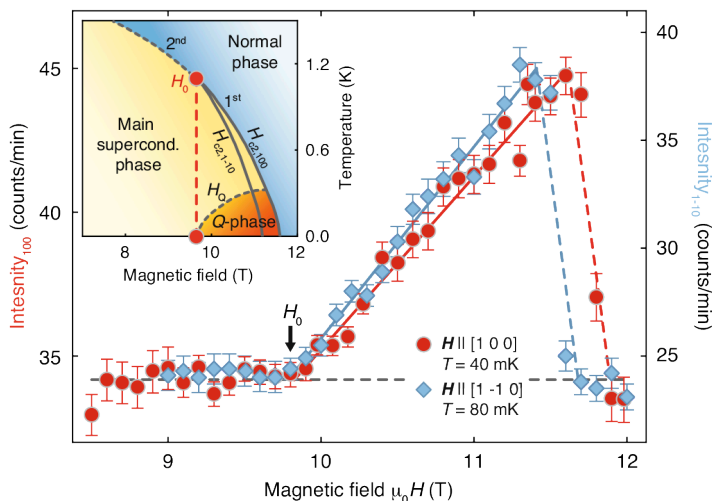


Fig. 1: Long-range SDW order emerges in the superconducting Q-phase of CeCoIn_5 close to the upper critical field H_{c2} , when external fields are applied within the tetragonal basal plane. Using neutron scattering the nature of magnetism can be probed directly by monitoring SDW Bragg peaks as a function of the field strength and direction. The Q-phase forms at a continuous quantum phase transition, hinting a magnetically-driven QCP inside the superconducting phase at $H_0(0)$. The onset-field also coincides with the field strength H_0 , where the superconducting transition becomes first-order and anisotropic (taken from [19]).

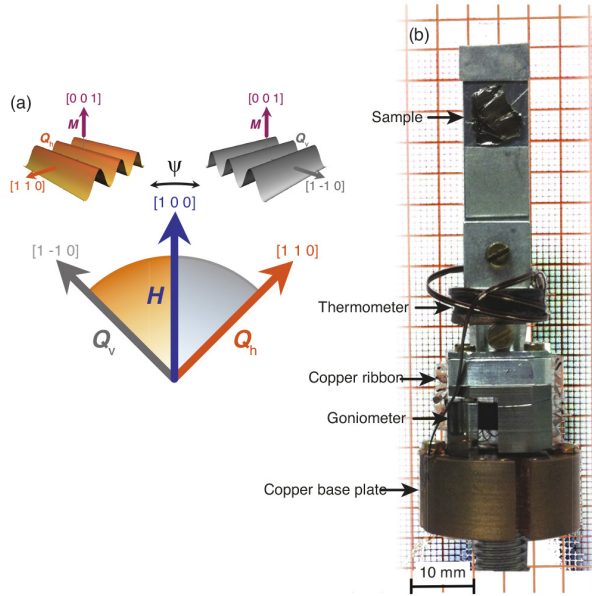


Fig. 2: (a) As a consequence of the symmetry constraints in the Q -phase only two SDW structures are allowed. Both have transversally-modulated magnetic moments $\mathbf{M} \parallel [0\ 0\ 1]$, but they propagate along orthogonal directions. For $\mathbf{H} \parallel [1\ 0\ 0]$ both domains are degenerate. (b) To carefully alter the magnetic field direction and measure the switching behavior of the SDW domains we built a non-magnetic piezo-electric sample rotator. Operating temperatures down to $T = 100$ mK at magnetic fields up to $\mu_0 H = 12$ T are achieved by connecting the rotator to a dilution refrigerator inside a cryomagnet (modified from [19]).

incommensurate SDW $\mathbf{Q} = (q, q, \frac{1}{2})$ in the presence of an external magnetic field \mathbf{H} parallel to the node and the full gap direction of the $d_{x^2-y^2}$ -wave superconducting order parameter. For $\mu_0 H > H_0 \approx 9.8$ T a continuous, linearly increasing magnetic signal is found up to H_{c2} , where magnetism and superconductivity break down simultaneously. Thus, magnetic order forms only within the superconducting phase.

A low-energy quasiparticle density of states with the same H -dependence was

identified using nuclear magnetic resonance [32] and taken as evidence for normal state paramagnetic particles. Therefore, our neutron scattering data suggests that the onset of SDW order arises simultaneously with a continuous transition that affects the electronic spectrum, concurrently implying that a novel magneto-superconducting quantum critical point is located at $H_Q(0)$, where magnetism and the paramagnetic charge carriers are directly linked [19].

SWITCHING OF MAGNETIC DOMAINS IN THE Q-PHASE

A real space representation of the two SDW structures that are allowed by the symmetry constraints in the Q -phase are shown in Fig. 2a. Both comprise transverse-amplitude modulated magnetic moments $\mathbf{M} \parallel [0\ 0\ 1]$, but propagate along orthogonal directions $[1\ 1\ 0]$ and $[1\ -1\ 0]$. Surprisingly, our measurements show that always only one mono-domain is populated and that the SDW propagation is pinned to $d_{x^2-y^2}$ -wave node that is *more* perpendicular to \mathbf{H} , where low-energetic quasiparticles permit electron nesting [19]. However, the domain imbalance cannot be explained by magnetic spin anisotropies as H

is applied perpendicular to the SDW moments.

For $\mathbf{H} \parallel [1\ 0\ 0]$, the two SDW domains are degenerate with equal components parallel to the magnetic field, the $d_{x^2-y^2}$ -wave superconducting order parameter and the crystal structure. Therefore, one may wonder whether the domain population can be tuned via the direction of \mathbf{H} . Figure 2b shows the purpose-built piezoelectric sample rotator that we conceived to carefully rotate the crystal lattice with respect to \mathbf{H} and determine the switching field direction.

The integrated Bragg peak intensity of the Q_h - and Q_v -domains, normalized to the averaged respective full population as a function of the angle ψ towards $[1\ 0\ 0]$ are shown in Fig. 3. Our data reveal that the domain

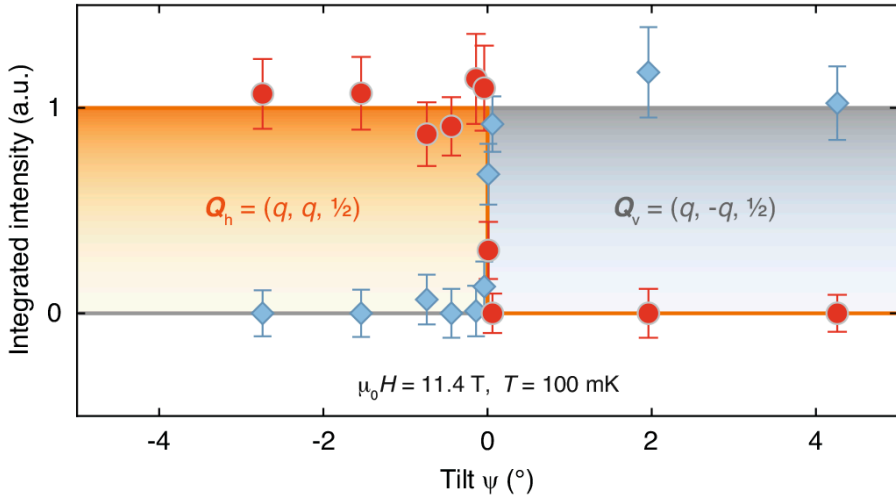


Fig. 3: (a) Domain population of the Q_h - (red circles) and the Q_v -domain (blue diamonds) as a function of the tilt angle ψ between the magnetic field direction H and the crystallographic $[1\ 0\ 0]$ direction. For $|\psi| \geq 0.05^\circ$ a mono-domain population is observed that can be macroscopically switched in a hypersensitive transition (taken from [19]).

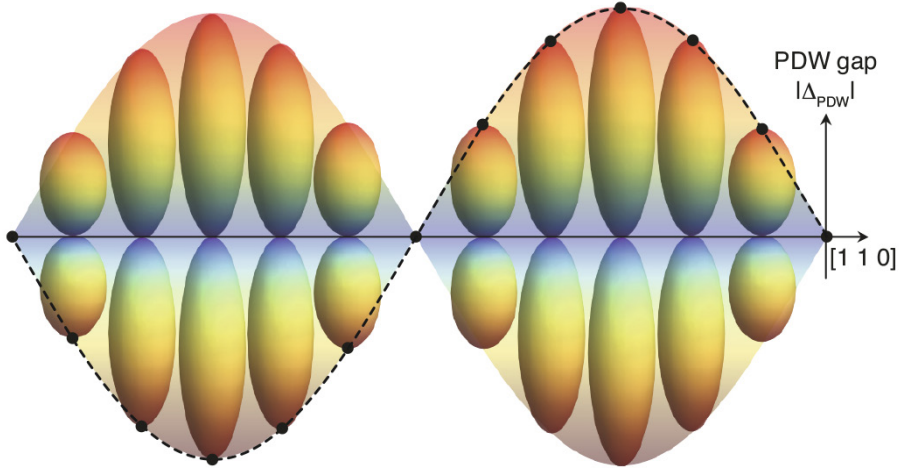


Fig. 4: Real space representation of the triplet Cooper pair-density wave gap structure along the $[1\ 1\ 0]$ crystallographic direction for $\mathbf{H} \parallel [1\ -1\ 0]$ and a populated Q_n SDW domain. The PDW emerges as a result of the direct coupling of $d_{x^2-y^2}$ -wave superconductivity and incommensurate SDW order. It also accounts for the hypersensitive switching of the SDW close to $\mathbf{H} \parallel [1\ 0\ 0]$ (taken from [19]).

population can be fully switched within only $\Delta\psi \approx 0.1^\circ$ [19]. Thus, the magnetic field direction allows direct access and control of the complex quantum state and permits hypersensitive macroscopic manipulation of the Q -phase ground state via the control parameter of the associated quantum phase transition.

EVIDENCE FOR A SPATIALLY INHOMOGENEOUS COOPER PAIR-DENSITY WAVE

Phenomenologically it has been shown that incommensurate SDW order that is directly coupled to a singlet (d -wave) superconductor induces a so-called Cooper pair-density wave (PDW), an additional triplet (p -wave) com-

ponent [16, 26, 27]. The finite-momentum ($-Q \neq 0$) triplet PDW component naturally appears as a result of directly coupled $d_{x^2-y^2}$ -wave singlet superconductivity ($Q = 0$) and finite-momentum ($Q \neq 0$) incommensurate SDW order to conserve momentum, i.e., translational symmetry. Agterberg *et al.* [26] have derived possible coupling terms on the basis of the irreducible representations of the full space group of CeCoIn_5 and the experimentally observed SDW symmetry in the Q -phase. Data presented in Fig. 3 reveals that electron nesting is only observed for $\mathbf{H} \perp \mathbf{Q}$. However, theories that rely on a nodal nesting-driven domain imbalance [29, 30] do not easily explain the hypersensitivity of the mono-domain state around $[1\ 0\ 0]$, which would require a fine-tuning of

interactions. On the other hand, as described above a linear coupling term of d -wave superconductivity, SDW and PDW order provides a much simpler explanation for the binary domain switching behavior: if the direction of the SDW Q -vector and the nodal direction of the PDW are identical the two order parameters can naturally coexist (see Fig. 4). This scenario fits well with the emergence of paramagnetic quasi-particles [32], since some components of the magnetic susceptibility tensor of a triplet order parameter do not change compared to the normal phase. Our arguments are bolstered by the independent observation of a significantly enhanced spin susceptibility in the Q -phase, compared to the main $d_{x^2-y^2}$ -wave phase [22].

Therefore, the hypersensitive switching of the Q -phase domains provides evidence for the condensation of a spatially inhomogeneous Cooper pair-density wave, which emerges spontaneously with an incommensurate SDW at the quantum phase transition $H_Q(T)$. In the limit of zero temperature, this phase boundary line ends at a multi-component QCP, involving both superconducting and magnetic degrees of freedom – a novel magneto-superconducting quantum critical point.

CONCLUSIONS

Neutron scattering is uniquely suited to directly access the cooperative interplay of ordered magnetism and unconventional superconductivity in CeCoIn_5 . Our results reveal that the incommensurate SDW in the Q -phase is driven by electron nesting along the nodes

of the $d_{x^2-y^2}$ -wave superconducting order parameter and occurs always in form of a single SDW mono-domain. However, carefully changing the direction of the applied magnetic field allows to macroscopically and binary switch the domain population. More fundamentally our results show that the complex Q -phase ground state emerges in a quantum phase transition, where magnetic order and superconductivity are directly coupled. It is this direct coupling that leads to the condensation of a spatially inhomogeneous Cooper pair-density wave and also accounts for the observed hypersensitive switching behavior of the Q -phase domain population. A speculative outlook relates to the direct access of the complex quantum state by using the coherence of the superconducting component for encoding information and manipulating it via switching of the SDW domains.

ACKNOWLEDGEMENTS

We thank all members of the Laboratories for Neutron Scattering & Imaging and Developments & Methods at the Paul Scherrer Institut for their assistance and discussions. In particular, we would like to acknowledge Jonathan White, Markus Zolliker and Pascal Fouiloux. We thank Manfred Sigrist, Cristian Batista, Piers Coleman, Kazushige Machida and Ken-ichi Kumagai for discussions. Work presented here is based on neutron scattering experiments performed on the thermal neutron two-axis diffractometer D23 at the Institut Laue-Langevin, Grenoble, France and the cold neutron triple-axis spectrometer RITA-II

at the Swiss Spallation Neutron Source SINQ, Paul Scherrer Institut, Villigen, Switzerland. We acknowledge support from the Swiss NSF under Contract No. 200021-122054, 200020-140345, Fellowship No. P2EZP2_148737 and the NCCR MaNEP.

A.D.B. received support from NSERC, FQRNT and the Canada Research Chair Foundation. Work at LANL was performed under the auspices of the US DOE, Office of Basic Energy Sciences, Division of Materials Sciences and Engineering.

REFERENCES

- * sigerber@stanford.edu
 † michel.kenzelmann@psi.ch
- [1] N. D. Mathur *et al.*, *Nature* **394**, 39 (1998).
 - [2] P. Monthoux, D. Pines and G. G. Lonzarich, *Nature* **450**, 1177 (2007).
 - [3] P. Gegenwart, Q. Si, and F. Steglich, *Nature Phys.* **4**, 186 (2008).
 - [4] C. Petrovic *et al.*, *J. Phys.: Condens. Matter* **13**, L337 (2001).
 - [5] G. Knebel, D. Aoki, and J. Flouquet, *C. R. Physique* **12**, 542 (2011).
 - [6] J. D. Thompson and Z. Fisk, *J. Phys. Soc. Jpn.* **81**, 011002 (2012).
 - [7] R. Settai *et al.*, *J. Phys.: Condens. Matter* **13**, L627 (2001).
 - [8] N. J. Curro *et al.*, *Phys. Rev. B* **64**, 180514(R) (2001).
 - [9] R. Movshovich *et al.*, *Phys. Rev. Lett.* **86**, 5152 (2001).
 - [10] K. Izawa *et al.*, *Phys. Rev. Lett.* **87**, 057002 (2001).
 - [11] M. P. Allan *et al.*, *Nature Phys.* **9**, 468 (2013).
 - [12] C. Stock *et al.*, *Phys. Rev. Lett.* **100**, 087001 (2008).
 - [13] A. D. Bianchi *et al.*, *Science* **319**, 177 (2008).
 - [14] J. S. White *et al.*, *New J. Phys.* **12**, 023026 (2010).
 - [15] P. Das *et al.*, *Phys. Rev. Lett.* **108**, 087002 (2012).
 - [16] M. Kenzelmann *et al.*, *Science* **321**, 1652 (2008).
 - [17] M. Kenzelmann *et al.*, *Phys. Rev. Lett.* **104**, 127001 (2010).
 - [18] E. Blackburn *et al.*, *Phys. Rev. Lett.* **105**, 187001 (2010).
 - [19] S. Gerber *et al.*, *Nature Phys.* **10**, 126 (2014).
 - [20] A. Bianchi *et al.*, *Phys. Rev. Lett.* **91**, 187004 (2003).
 - [21] H. A. Radovan *et al.*, *Nature* **425**, 51 (2003).
 - [22] V. F. Mitrovic *et al.*, *Phys. Rev. Lett.* **97**, 117002 (2006).
 - [23] K. Kumagai *et al.*, *Phys. Rev. Lett.* **97**, 227002 (2006).
 - [24] Y. Matsuda and H. Shimahara, *J. Phys. Soc. Jpn.* **76**, 051005 (2007).
 - [25] B.-L. Young *et al.*, *Phys. Rev. Lett.* **98**, 036402 (2007).
 - [26] D. F. Agterberg, M. Sigrist, and H. Tsunetsugu, *Phys. Rev. Lett.* **102**, 207004 (2009).
 - [27] A. Aperis, G. Varelogiannis, and P. B. Littlewood, *Phys. Rev. Lett.* **104**, 216403 (2010).
 - [28] Y. Yanase and M. Sigrist, *J. Phys. Soc. Jpn.* **80**, 094702 (2011).
 - [29] K. M. Suzuki, M. Ichioka, and K. Machida, *Phys. Rev. B* **83**, 140503(R) (2011).
 - [30] Y. Kato, C. D. Batista, and I. Vekhter, *Phys. Rev. Lett.* **107**, 096401 (2011).
 - [31] Y. Hatakeyama and R. Ikeda, arXiv:1412.2898.
 - [32] K. Kumagai *et al.*, *Phys. Rev. Lett.* **106**, 137004 (2011).

Announcements

SGN/SSDN MEMBERS

Presently the SGN has 199 members. New members can register online on the SGN website: <http://sgn.web.psi.ch>

SGN/SSDN ANNUAL MEMBER FEE

The SGN/SSDN members are kindly asked to pay their annual member fees. At the general assembly 2013 of the society, the fee has been increased from CHF 10 to **CHF 20**. It can be paid either by bank transfer or in cash during your next visit at PSI. The bank account of the society is accessible for both Swiss national and international bank transfers. The coordinates are as follows: Postfinance: 50-70723-6 (BIC: POFICHBE), IBAN: CH39 0900 0000 5007 0723 6.

The SGN is an organization with tax charitable status. All fees and donations paid to the SGN are **tax deductible**.

SGN/SSDN GENERAL ASSEMBLY 2015

The SGN/SSDN General Assembly 2015 will be held in conjunction with the European Conference on Neutron Scattering (ECNS) held in Zaragoza, Spain, August 30th - September 4th, 2015.

PSI FACILITY NEWS

Recent news and scientific highlights of the three major PSI user facilities SLS, SINQ and μ S can be found in the **quarterly electronic newsletter** available online under: <http://www.psi.ch/info/facility-news>

SINQ CALL FOR PROPOSALS

The next deadline for the submission of beam time requests for the Swiss spallation neutron source 'SINQ' (<http://sinq.web.psi.ch>) is:

May 15, 2015

NEUTRON BEAM TIME AT SNS FOR THE SWISS NEUTRON COMMUNITY

An actively shielded 16 Tesla magnet has been realized at the Spallation Neutron Source SNS in Oak Ridge, USA, as a collaboration of the Swiss neutron community and SNS. In return, beam time is available at SNS for Swiss users. Swiss neutron scatterers are therefore encouraged to apply for beamtime at SNS.

REGISTRATION OF PUBLICATIONS

Please remember to **register all publications either based on data taken at SINQ, SLS, SpS or having a PSI co-author** to the Digital User Office: <https://duo.psi.ch>. Please follow the link 'Publications' from your DUO main menu.

OPEN POSITIONS AT ILL

To look for open positions at ILL, please have a look at the following webpage of ILL: <http://www.ill.eu/careers>

PHD POSITIONS AT ILL

The PhD program of the Institut Laue-Langevin, ILL, is open to researchers in Switzerland. The contact person at ILL is Anne-Claire Dupuis (PhD@ill.eu). The Swiss agreement with the ILL includes that ILL funds and hosts one PhD student from Switzerland.

Minutes of the SGN/SSDN General Assembly 2014

Date/Location: *November 26, 2014, Paul Scherrer Institut, main auditorium*
Start: *18:00*
End: *19:00*
Participants: *7 members of the society*

1. WELCOME

As the president of the SGN/SSDN, Henrik Ronnow, is on sabbatical leave, board member Urs Gasser welcomes the participants to the general assembly 2014.

2. MINUTES OF THE GENERAL ASSEMBLY 2013

The minutes of the general assembly of the SGN/SSDN from 13.11.2013, published in Swiss Neutron News #43 are accepted without objections.

3. ANNUAL REPORT OF THE CHAIRMAN

U. Gasser reports on the activities of the SGN/SSDN in the year 2014:

- a) The inaugural Young Scientist Prizes of the SGN/SSDN sponsored by Swiss Neutronics have been awarded to Dr. Simon Gerber and Dr. Qianli Chen. As Swiss Neutronics is sponsoring the Young Scientist Prize, it is planned to award it every year, not every second year as decided at the general assembly in 2013.
- b) As of Nov. 2013, the SGN has tax charitable status. The membership fees and donations are tax deductible.
- c) Two new issues of Swiss Neutron News have appeared in March and August 2014.
- d) The SGN/SSDN has presently 199 members.

4. REPORT OF THE TREASURER

The annual balance sheet 2013 is presented:

Assets SGN/SSDN on 1.1.2013: **SFr 3929.44**

	Revenues [SFr]	Expenses [SFr]
Membership-fees (cash box)	200.00	
Membership-fees (postal check acc.)	480.00	
Donations (cash box)	55.00	
Interest	1.95	
Expenses PC account		42.85
Apero Zuoz		602.00
Total	736.95	644.85
Net earnings 2013:	SFr 92.10	
Assets SGN/SSDN on 31.12.2013:	SFr 4021.54	

Balance sheet 2013:	Assets [SFr]	Liabilities [SFr]
Postal check account	3811.54	
Cash box	210.00	
Assets on 31.12.2013	4021.54	

5. REPORT OF THE AUDITORS

Bericht der Revisoren

Die Rechnungsrevisoren haben die Belege, die Abrechnungen und die Bilanz für das Jahr 2013 geprüft und für in Ordnung befunden!

			
Datum	Dr. M. Zolliker, PSI	Datum	Dr. K. Krämer, Uni Bern

Both Auditors (K. Krämer and M. Zolliker) have examined the bookkeeping and the balance 2013. They have accepted it without objection. The participants therefore unanimously vote for a release of the SGN/SSDN board.

6. BUDGET 2015

Urs Gasser presents the following proposal for the budget 2015:

	Receipts [SFr]	Expenditures [SFr]
member fees	800.00	
interest	0.00	
fees PC account		40.00
Summer School aperitif 2015		600.00
<hr style="border-top: 1px dashed black;"/>		
Total	800.00	640.00
balance 2014	160.00	
<hr style="border-top: 1px dashed black;"/>		

The participants accept the budget proposal unanimously.

7. NEWS FROM ENSA (H. RONNOW)

Urs Gasser relays H. Ronnow's news from ENSA.

- a) The last ENSA meeting took place in Munich, Germany (June, 2014). The term of Michael Steiner as the chairman of ENSA has ended in 2014. Christiane Alba-Simionescu (LLB, France) was elected as the new chairperson, and Ferenc Mezei (ESS) has become the new vice-chairman.
- b) ENSA is still in the process to find its role to support both neutron users and neutron facilities in all of Europe. With the clear commitment of Europe for ESS and Christiane Alba-Simionescu as new chairperson, ENSA is expected to have new momentum to redefine its role.
- c) Concerning the future European neutron landscape including ESS, sacrifices at other neutron sources may have to be made

when ESS becomes operational. Where and how such sacrifices should / could be made needs to be discussed. Suggestions regarding this issue are welcome!

- d) The next European Conference on Neutron Scattering (ECNS) will be organized in Zaragoza, Spain, August 30th – September 4th, 2015.

8. NEWS FROM ILL (CH. RÜEGG)

Christian Rüegg as the Swiss representative in the ILL Scientific Council (SC) reports on the 89th Scientific Council meeting:

- a) After difficult negotiations between ILL and Switzerland, a new contract has been signed. Switzerland will continue to contribute about 3M CHF per year. The mode of calculation for beamtime has become increasingly unfavorable for Swiss users; it is to be expected that more proposals will be refused due to national beamtime quota.

- b) To improve the access to ILL for Swiss users, it is planned to get access to the collaborating research group (CRG) instruments of the CEA. The CEA operates the instruments IN22, IN12, and D23. A contract for a Swiss participation in these instruments is being negotiated between EPFL and CEA.
- c) As the 3rd “Millennium” program, ILL plans to start the program “Endurance” in 2015. The volume of this is planned to be about 50 M \leftrightarrow , but the funding is not yet secured. About 10 instruments will be upgraded.
- d) Recently, a new instrument has been completed: Thales (the new IN14). Until the end of 2015, WASP the new high-intensity spin-echo spectrometer is expected to become operational.
- e) In 2014, the SC has been restructured. Ch. Rüegg represents Switzerland and acts as vice chairman.

9. NEWS FROM SINQ (CH. RÜEGG)

- a) In 2014, SINQ has received 438 new proposals, about 10% more than in 2013. The number of experiment days in 2013, 1841, was somewhat lower than in 2012 with 2086 due to the relatively large number of beam failures. Accordingly, the number of visits in 2013, 870, was also lower than in 2012 (1001).
- b) 51% of the beam time in 2013 was used by Swiss users. The largest Swiss user groups are PSI (62%), EPFL (15%), and ETH Zürich (11%).
- c) As SwissFEL and SLS have obtained the priority for large upgrades at PSI, the up-

grade program for SINQ, SINX², has been postponed. Smaller upgrades of the SINQ source and selected instruments will be realized in the timeframe from 2015 to 2024.

- d) All instruments at SINQ can profit from an upgrade of the neutron guide system, which is estimated to cost about 12M CHF. However, the funding for this project is unconfirmed.
- e) Upgrades for two SINQ instruments have been founded. The cold triple-axis spectrometer Rita-II will obtain the new multi-analyzer CAMEA, which is funded by the SNF, EPFL, and PSI. The single-crystal diffractometer Trics will be replaced by ZEBRA, which will be optimized for small samples and extreme conditions. This upgrade is funded by SNF, UniFR, and PSI.

10. NEWS FROM ESS (CH. RÜEGG)

- a) The European Spallation Source (ESS) is now under construction in Lund, Sweden, and is planned to become operational in 2019. Switzerland is among the 17 member countries and contributes 3.5% to the construction budget of 1.8B € .
- b) The Swiss neutron scattering community has submitted five proposals for future instruments at ESS in collaboration with Denmark and Germany. Three of the Swiss-Danish proposals have been approved for construction by the Scientific Advisory Committee and the Steering Committee of ESS. These are the extreme environment spectrometer CAMEA, the focusing reflectometer ESTIA-SELENE, and the diffractometer HEIMDAL. The Swiss-German pro-

posal for the neutron imaging instrument ODIN has also been accepted for construction. Furthermore, Switzerland is involved in the design of the neutron source with neutron optics and neutron background simulations.

11. THE NEUTRON LANDSCAPE

(K. CLAUSEN)

Kurt Clausen gives a report about the last meeting of the European Strategy Forum on Research Infrastructure (ESFRI) of the European Union, which was held in Trieste 24 Sept. 2014. Switzerland is represented by the Swiss Secretariat for Research and Innovation. A call for proposals for new facilities to be included in the next ESFRI large-scale facility road map was launched at the meeting. ESFRI has established a number of science working groups to follow and review proposals for new facilities. R. Abela and K. Clausen are members of the Physical Science and Engineering Work Group (PSE-WG).

- a) ESFRI works with a 10-year roadmap for European research infrastructure projects. Every project on the roadmap needs the support of at least three member countries and needs to be advanced enough to move to implementation within 10 years. A new roadmap is being defined in January 2016.
- b) As ESS is now in the construction phase, no neutron sources are on the current ESFRI roadmap.
- c) The PSE-WG has the task to prepare a landscape document of the large scale facilities in Europe and to identify any present or future gaps.

- d) It is expected that the number of available experiment days at neutron scattering facilities in Europe will decrease after about 2020, as several facilities will be closed. Only a partial recovery is expected towards 2030, when ESS is expected to operate 22 instruments. Therefore, the strategy should be to build ESS and to keep current neutron infrastructures running and up to date for at least the next 15 years to meet the need of European researchers in the long term.
- e) It is expected that several continuous wave neutron sources (research reactors) will be closed without replacement. SINQ is expected to be one of the few continuous wave sources available in Europe.

12. MISCELLANEOUS

- a) P. Fischer asks about the strategy of PSI regarding SINQ. K. Clausen answers: The SINQ target has been optimized; a further significant increase in neutron flux cannot be expected. However, it is possible to realize substantial gains by upgrading the neutron guides and the instruments. For the time after about 2025, PSI will have to decide about the future of the proton accelerator HIPA, which is the oldest and most expensive of the large facilities of PSI but is expected to remain a very competitive facility.
- b) P. Fischer recommends to organize the next SGN general assembly in conjunction with another neutron scattering event.

U. Gasser
January 2015

Conferences and Workshops 2015 and beyond

(an updated list with online links can be found here:
<http://www.psi.ch/useroffice/conference-calendar>)



APRIL 2015

- Memorial Seminar - Fyodor L. Shapiro
April 6-7, 2015, Dubna, Russia
- 1st CSSB International Symposium "Systems in Infection Biology - From Molecules to Organisms"
April 9-11, 2015, Hamburg, Germany
- MPS 2015: Membrane Protein Structures 2015 Meeting and one-day workshop on Membrane Protein Technologies
April 9-12, 2015, Lemont, USA
- Corrosion Chemistry: Faraday Discussion
April 13-15, 2015, London, UK
- cost2015: School on Interfacial Science and Colloidal Chemistry.
April 13-16, 2015, London, UK
- Advanced School in Soft Condensed Matter 'Solutions in the Spring'
April 13-16, 2015, Loughborough, UK
- Structural Systems Biology - From Molecules to Organisms
April 13-17, 2015, Hamburg, Germany
- canSAS-VIII: Collective Action for Nomadic Small Angle Scatterers
April 14-16, 2015, Tokai, Japan
- Crystallisation & Polymorphism for Discovery Chemists
April 16, 2015, Cambridge, UK
- 56th Experimental Nuclear Magnetic Resonance Conference
April 19-24, 2015, Pacific Grove, USA
- Crystallography for the next generation: the legacy of IYCr
April 22-24, 2015, Rabat, Morocco
- Dielectrics 2015
April 22-24, 2015, Teddington, UK
- AnalytiX-2015. BIT's 4th Annual Conference and EXPO
April 25-28, 2015, Nanjing, China

- ICDD Clinics on practical X-ray fluorescence, April 27 - May 1, 2015, Newtown Square, USA

MAY 2015

- RapiData 2015. Data Collection & Structure Solving. A Practical Course in Macromolecular X-ray Diffraction Measurement May 3-8, 2015, Stanford, USA
- Canadian Light Source 18th Annual Users' Meeting and Related Workshops May 4-6, 2015, Saskatoon, Canada
- EMBO Global Exchange Lecture Course on 'Structural and biophysical methods for biological macromolecules in solution' May 4-10, 2015, Taipei, Taiwan
- International conference: Multi-Pole Approach to Structural Science May 10-13, 2015, Warsaw, Poland
- 2015 APS/CNM Users Meeting May 11-14, 2015, Lemont, USA
- 2015 E-MRS Spring Conference & Exhibit May 11-15, 2015, Lille, France
- PolyChar 23. 23rd World Forum on Advanced Materials May 11-15, 2015, Lincoln, USA
- UCANS V: 5th International Meeting of Union for Compact Accelerator - Driven Neutron Sources May 12-15, 2015, Legnaro (Padova), Italy
- Self-Assembly & Supramolecular Chemistry. Gordon Research Seminar May 16-17, 2015, Lucca (Barga), Italy
- Self-Assembly & Supramolecular Chemistry. Gordon Research Conference May 17-22, 2015, Lucca (Barga), Italy
- EMBO workshop: Small angle neutron and X-ray scattering from proteins in solution May 18-22, 2015, Grenoble, France
- School on Modern Methods in Rietveld Refinement for Structural Analysis May 19-21, 2015, Tallahassee, FL, USA
- NASSCC-2015: North American Solid State Chemistry Conference May 22-24, 2015, Tallahassee, FL, USA
- Superconductivity - Unconventional Superconductivity: Materials and Mechanisms May 24-29, 2015, Hongkong, China
- Total Scattering for Nanotechnology on the Como Lake May 25-28, 2015, Como, Italy
- MaMaSELF Status Meeting 2015 May 26-29, 2015, Rigi Kulm, Switzerland
- DMI 2015: 3rd International Workshop on Dzyaloshinskii-Moriya Interaction and Exotic Spin Structures May 26-29, 2015, Pskov, Russia

JUNE 2015

- 6th Workshop on Neutron Scattering Applications in Structural Biology June 1-5, 2015, Oak Ridge, TN, USA
- 48th Erice Course: Engineering Crystallography: from Molecule to Crystal to Functional Form June 5-14, 2015, Erice, Sicily, Italy
- ISFRS 2015: The 7th International Symposium on Food Rheology and Structure June 7-11, 2015, Zurich, Switzerland
- International Conference on Applied Mineralogy and Advanced Materials June 7-12, 2015, Taranto, Italy

- XVIII SAGAMORE Conference on Charge Spin and Momentum Densities
June 7-12, 2015, Santa Margherita di Pula (CA), Sardinia, Italy
 - The Zurich School of Crystallography: bring your own crystals
June 7-20, 2015, Zurich, Switzerland
 - Summer School on Methods and Applications of Neutron Spectroscopy
June 8-12, 2015, NIST, Gaithersburg, MD, USA
 - Learning Days of the Italian Society of Neutron Spectroscopy 2015
June 13-22, 2015, S. Giovanni Valle Auri-
na, Italy and Grenoble, France
 - 17th Annual US School on Neutron and X-
ray Scattering
June 13-27, 2015, Oak Ridge, TN, USA
 - DSE 2015: 100 Years of the Debye Scatter-
ing Equation
June 14-18, 2015, Cavalese, Italy
 - BioStruct-X Industrial Workshop
June 15-17, 2015, Hamburg, Germany
 - VII AUSE meeting and II ALBA user's meeting
June 16-19, 2015, Cerdanyola del Valles
near Barcelona, Spain
 - ISIS Neutron training course
June 16-25, 2015, Abingdon, UK
 - Public Awareness of Research Infrastruc-
tures
June 18-19, 2015, Garching, Germany
 - Gordon Research Conference on Neutron
Scattering: A Powerful Tool for Materials
Research and Industrial Development
June 21-26, 2015, Hong Kong, China
 - Structure and dynamics of polymer nano-
composites
June 22-24, 2015, Montpellier, France
 - DSL 2015: 11th International Conference
on Diffusion in Solids and Liquids
June 22-26, 2015, Munich, Germany
 - ZMPC 2015: International Symposium on
Zeolites and MicroPorous Crystals
June 28 - July 2, 2015, Sapporo, Japan
 - Topological and Correlated Matter - Ad-
vances in Topological Phases of Matter in
Crystalline Solids and Cold Atom Systems
June 28 - July 3, 2015, Hongkong, China
 - 5th European PEFC and H2 Forum
June 30 - July 3, 2015, Lucerne, Switzer-
land
- JULY 2015**
- ICM2015: 20th International Conference
on Magnetism
July 5-10, 2015, Barcelona, Spain
 - 2015 Asia-Pacific Edition of HERCULES in
TAIWAN
July 6-24, 2015, Hsinchu, Taiwan
 - AOCNS-2015: 2nd Asia Oceania Confer-
ence on Neutron Scattering
July 19-23, 2015, Sydney, Australia
 - ACA2015: American Crystallographic As-
sociation Annual Meeting
July 25-29, 2015, Philadelphia, PA, USA
 - XIII edition of the School on Neutron Scat-
tering 'Francesco Paolo Ricci'
July 28 - August 4, 2015, Erice, Italy
- AUGUST 2015**
- PSI Summer School on Condensed Matter
Research 2015
August 15-21, 2015, Zuo, Switzerland

- Diffusion Fundamentals VI
August 23-26, 2015, Dresden, Germany
- M2S 2015: 11th International Conference on Materials and Mechanisms of Superconductivity
August 23-28, 2015, Geneva, Switzerland
- ECM29: The 29th European Crystallographic Meeting
August 23-28, 2015, Rovinj, Croatia
- XAFS16: 16th International Conference on X-ray Absorption Fine Structure
August 23-28, 2015, Karlsruhe, Germany
- Structural Biology on the Move
August 24-27, 2015, Copenhagen, Denmark
- ECNS2015: VI European Conference on Neutron Scattering
August 30 - September 4, 2015, Zaragoza, Spain

SEPTEMBER 2015

- 14th Oxford School on Neutron Scattering
September 6-18, 2015, Oxford, UK
- SRPS6: VI International Conference of Synchrotron Radiation in Polymer Science
September 7-10, 2015, Madrid, Spain
- ISCOM 2015: 11th International Symposium on Crystalline Organic Metals, Superconductors and Magnets
September 7-11, 2015, Bad Gögging, Germany
- 19th JCMS Laboratory Course Neutron Scattering
September 7-18, 2015, Jülich and Garching, Germany
- GISAS 2015: 3rd International GISAS Conference
September 8-11, 2015, Nice, France

- SAS2015: 16th International conference on Small-Angle Scattering
September 13-18, 2015, Berlin, Germany
- Annual Meeting and General Assembly 2015 of the Swiss Society for Crystallography SGK/SSCr
September 14, 2015, Neuchatel, Switzerland
- XXIII Conference on Applied Crystallography
September 20-24, 2015, Krynica Zdroj, Poland
- Autumn School for Neutron Imaging
September 28 - October 2, 2015, PSI Villigen, Switzerland

OCTOBER 2015

- 2nd International Conference on Rheology and Modeling of Materials
October 5-9, 2015, Lillafured, Hungary
- NMI3-II: General Assembly 2015
October 14-16, 2015, Copenhagen, Denmark

NOVEMBER 2015

- 2015 MRS Fall Meeting and Exhibit
November 29 - December 4, 2015, Boston, MA, USA

AUGUST 2016

- Neutron Powder Diffraction School 2016
August 22-26, 2016, Villigen, Switzerland
- ECM-30: European Crystallographic Meeting
August 28 - September 1, 2016, Basel, Switzerland

Swiss Neutron Scattering Society

Sekretariat SGN/SSDN

Paul Scherrer Institut

WLGA/018

5232 Villigen PSI, Switzerland